FLOW VISUALIZATION STUDY OF THE INLET VORTEX PHENOMENON

by

FRANCESCA DE SIERVI

B.E., The Cooper Union
(June 1979)

SUBMITTED IN PARTIAL FULFILLMENT
OF THE REQUIREMENTS FOR THE
DEGREE OF

MASTER OF SCIENCE

at the

MASSACHUSETTS INSTITUTE OF TECHNOLOGY

May 1981

Signature of Author _____

Department of Mechanical Engineering
May 19, 1981

Certified by _____

Edward M. Greitzer
Thesis Supervisor

Accepted by _____

Warren M. Rohsenow
Chairman, Department Committee

A FLOW VISUALIZATION STUDY OF THE INLET VORTEX PHENOMENON

by

Francesca De Siervi

Submitted to the Department of Mechanical Engineering on May 19, 1981, in partial fulfillment of the requirements for the Degree of Master of Science in Mechanical Engineering

ABSTRACT

The inlet vortex phenomenon was experimentally investigated in a water tunnel, using hydrogen bubble flow visualization techniques. Several inlet ambient flow configurations were studied, including an inlet-ground plane configuration, in a known shear as well as irrotational flow, and a double inlet configuration in irrotational flow only. This latter situation created a boundary layer free analogue of the ground plane and enabled the investigation of the inlet vortex formation in flow essentially free of ambient vorticity. The three dimensional inlet flow field and vortex formation mechanisms were determined by marking material lines and observing their path and deformation as they are convected from a far upstream location into the inlet.

Two basic mechanisms of inlet vortex generation were found. For flows possessing ambient vertical vorticity, the amplification of this vorticity as the vertical vortex lines are stretched and drawn into the inlet results in the formation of an inlet vortex. However, an inlet vortex does not require the presence of ambient vorticity to form. It can also be created in irrotational flow, with an inlet in crosswind. In this situation, it is accompanied by a variation in circulation along the axial length of the inlet lip region. The ratio of inlet velocity to upstream velocity is an important parameter in determining the generation of an inlet vortex for both mechanisms.

Thesis Supervisor: Dr. Edward M. Greitzer
Associate Professor of Aeronautics *and Astronautics*

ACKNOWLEDGEMENTS

First and foremost the author would like to express her deep appreciation and respect for her thesis advisor, Professor E.M. Greitzer. His guidance was essential to the completion of this report and his constant encouragement and accessibility made working on it a pleasure. Special thanks are also due to Dr. C.S. Tan whose advice was indispensable in all phases of the research. His generous sharing of time, especially during the hectic experimental phase of this work, also deserves acknowledgement.

The author would also like to express her appreciation to Professor F.E. Marble for taking the time to discuss the problem and for his insight into its solution. Professor E.E. Covert also deserves her thanks for his many helpful recommendations throughout the course of this work. In addition, the suggestions of Professor A.H. Epstein on experimental technique, especially in relation to lighting, were invaluable and sincerely appreciated.

Dr. N.A. Cumpsty (Cambridge University) also deserves mention. He sparked the investigation that revealed the new mechanism of vortex formation described herein through his stimulating (albeit erroneous) appraisal of the phenomenon.

The author is also grateful to all the members of the Gas Turbine Laboratory and to all her friends at M.I.T. for making the last two years an enjoyable experience that she will remember and treasure always.

The typing skills of Barbara Rosen are also appreciated.

Finally, the author would like to dedicate this thesis to her family, expecially her parents, whose love and unending support were constantly felt across the miles.

This research was supported by the Air Force Office of Scientific Research under Contract No. F49620-78-C-0084, Dr. J.D. Wilson, Program Manager.

TABLE OF CONTENTS

LIST OF FIGURES

Figure Number

Figure Number

22a High Value of U_i/U , Symmetric Separation

22b First Intermediate Value of U_i/U , Asymmetric Separation is Beginning

22c Second Intermediate Value of U_i/U , Asymmetric Separation Evident

22d Low Value of U_i/U , Inlet Separation at 4:00

Fig. 23 90^o Inlet in Transient Irrotational Upstream Flow (Photograph of Hydrogen Bubble Flow Visualization)

Fig. 24 Streamlines Associated with 90^o Double Inlet Configuration in Irrotational Upstream Flow (Drawn from Hydrogen Bubble Flow Visualization)

Fig. 25 Vortex Lines Associated with 90^o Double Inlet Configuration in Irrotational Upstream Flow (Drawn from Hydrogen Bubble Flow Visualization)

Fig. 26 Material Lines Associated with 90^o Double Inlet Configuration in Irrotational Upstream Flow (Drawn from Hydrogen Bubble Flow Visualization)

Fig. 27 Material Lines Associated with 90^o Double Inlet Configuration in Irrotational Upstream Flow (Photograph of Hydrogen Bubble Flow Visualization)

Fig. 28 Vortex Core Extending Between Two 90^o Inlets in Irrotational Upstream Flow (Photograph of Hydrogen Bubble Flow Visualization)

Fig. 3-1 Hydrogen Bubble Flow Visualization DC Circuit

LIST OF SYMBOLS

D	Inlet Inside Diameter
d	Hydrogen Bubble Diameter
H	Height of Inlet Centerline Above the Ground Plane
g	Gravity
CW	Clockwise
CCW	Counterclockwise
p_∞	Upstream Pressure
p_D	Pressure Downstream of Honeycomb
$p(o,s)$	Pressure Just In Front of Honeycomb
f	Friction Factor of Honeycomb
L	Length of Honeycomb
D_h	Hydraulic Diameter of Honeycomb
ρ	Density of Water
U_i	Inlet Velocity
$U(s)$	Velocity Profile
U_∞	Free Stream Velocity
$\underline{V}$	Velocity Vector
s	Direction in Which Velocity Profile Varies
ψ	Stream Function
ℓ	Tunnel Height
x	Axial Tunnel Direction
u	Velocity Component in x Direction
v	Velocity Component in s Direction
K_o	Flow Pressure Coefficient

Re	Reynolds Number
ν	Kinematic Viscosity of Water
β	Open Area to Total Area Ratio of the Honeycomb
$\underline{\omega}$	Vorticity Vector

CHAPTER 1

INTRODUCTION

The inlet vortex phenomenon has been of interest for some time, in connection with the gas turbine engine operation near a ground plane. In this situation, a strong vortex can form and be ingested into the engine inlet. The flow is often made visible "naturally" by water vapor condensing in the high-velocity and low-temperature center of the swirling region. In the past, the phenomenon's notoriety was mainly due to its ability to lift and ingest foreign matter into the engine. Although the damage thus incurred can be significant, a more serious potential threat is that the vortex creates a compressor inlet velocity distortion that can induce compressor surge. Recently, the formation of inlet vortices has become more prevalent due to the advent of wide-body aircraft with high bypass ratio engines which possess larger diameter engines at a closer proximity to the ground. In these engines, the inlet vortex also can encompass a larger proportion of the primary air stream; therefore, its impact on the core compressor is more severe.

The inlet vortex produces a swirling flow which has a large amplitude, large extent, flow angle and velocity distortion, but often a small extent total pressure defect. Thus it cannot be predicted by present distortion analyses which are aimed at roughly uni-directional flow with large amplitude total pressure

defects over a significant extent of the compressor. Previous studies have dealt with this phenonmenon qualitatively. In particular, a basic explanation has not been given either for the mechanisms that generate the inlet vortex or for the predominant characteristics of the flow field. A detailed examination of this flow field especially in the region of the engine inlet is therefore necessary to understand the salient features of this complicated flow.

This thesis summarizes an experimental investigation of the fluid mechanics of the ground vortex. The experiment was conducted in a large water tunnel using hydrogen bubble flow visualization. Both steady flow and transient studies were carried out with a single inlet configuration (similar to the actual physical geometry of the situation) as well as with a double inlet configuration. The tests provided an understanding of the overall three dimensional inlet velocity field and of the two basic mechanisms associated with the generation of an inlet vortex.

The single inlet was examined in a known shear flow as well as in an irrotational flow, the former being created by honeycomb of non-uniform lengths. For the shear flow, the convection downstream and ingestion of the vortex lines, which are material lines in the flows studied, could be observed using hydrogen bubbles, since a line of hydrogen bubbles is a good approximation of a material line. Two types of material lines were studied in detail: those initially

parallel to the ground and normal to the mean flow far upstream, and those vertical and normal to the flow far upstream. For each case, the inlet was positioned at zero degrees and ninety degrees relative to the mean upstream flow; the latter case modelling a crosswind condition. In addition to the zero degree and ninety degree inlet orientation, the irrotational flow case was also investigated at two hundred and seventy degrees to the upstream flow.

The double inlet configuration was examined in irrotational flow only with inlet orientations to the mean flow of zero degrees, ninety degrees, and two hundred and seventy degrees. In this case, the ground plane was replaced by an (inviscid) plane of symmetry between the two inlets. The vortices obtained with this configuration thus precluded any speculation that the ingestion of a ground boundary layer is necessary for their formation. In addition, it enabled the examination of the inlet vortex generation with completely irrotational flow upstream of the inlet.

During the investigation, a previously undetected feature of the flow field around an inlet at ninety degrees to the mean upstream flow was revealed. A large vortex trailed from the downstream side of the inlet. Associated with this vortex was a shift in the separation points on the inlet at the lip. This new feature was examined for steady and transient flow conditions and its relation to the inlet vortex formation was described.

CHAPTER 2

BACKGROUND

Many studies of the inlet vortex phenomenon have been conducted in the past. However, a detailed summary of previous investigations can be found in reference (1), and we will therefore only discuss the main conclusions shown by these studies. There are several dominant characteristics of this phenomenon that are described. First, it is assumed that an inlet vortex can form only if ambient vorticity exists in the fluid drawn into the engine. Second, a stagnation point on the ground appears to be necessary. Third, the existence of the (thin) boundary layer due to the sink flow created by the inlet is not believed to be vital. Fourth, the essential parameters needed to describe this phenomenon are believed to be the inlet velocity to wind velocity ratio, the center-line height to the inlet diameter ratio, the inlet velocity to the product of the wind velocity gradient and inlet diameter ratio, and the wind direction. Fifth, a stagnation point forms under near-static conditions; however, if the wind velocity is too high it will blow away and a vortex will not form.

In spite of the work that has been done on this topic, the basic features of the inlet flow and the mechanisms that generate it are still not completely understood. For example, if we accept the hypothesis that the formation of the inlet vortex is due to the intensification of ambient vorticity as

it is ingested into the inlet, the evolution of the far upstream vortex lines into the inlet must appear as sketched in Figure 1 which shows a sketch of a vortex line at three instants of time. Since the vortex lines cannot end in the fluid, the two legs that are ingested should each possess vorticity with equal and opposite circulation. However, only one vortex appears to have been observed in previous studies.

Some insight into the solution of this basic question is rendered by Viguier in reference (1). In this report, a secondary flow approach is implemented to study this phenomenon. The flow is assumed to consist of a weak shear flow and a mean irrotational primary flow with the vortex lines associated with the former being regarded as convected by the latter. The amplification of the vorticity can be found by computing the stretching of the vortex lines. This is done by "tracking" two particles between a far upstream location where the vorticity is known and the engine inlet. For vortex lines initially vertical and perpendicular to the mean flow, Viguier found that the upper legs of the vortex lines are fanned out over the upper part of the inlet while the lower legs are squeezed around the forward stagnation line. The central concept is shown in Figure 2 which is taken from (1) and is for an engine with a headwind, i.e. oriented at zero degrees to the mean flow. The verification of these results and the location of the second vortex "leg" in crosswind are two prospective goals of the present investigation.

A second fundamental question deals with the possibility of an inlet vortex forming in irrotational flow, i.e. in the absence of ambient vorticity. Anticipating the experimental results to be discussed subsequently, we can mention that contrary to what has been supposed an inlet vortex can form in a uniform (far upstream) flow. The mechanism of its formation, which is new and has not been previously discussed, is also explored in this study.

CHAPTER 3

FLOW FIELD DESCRIPTION

3.1 THE ACTUAL FLOW

The three dimensional flow field actually produced by a jet engine run in proximity to the ground is very complex. To investigate the structure of this flow field, the fluid is assumed to be incompressible and steady with negligible body forces. In addition, it is expected that viscous effects will not be significant over the major part of the volume of the flow field. Typically, the Reynolds number based on center-line height and approaching wind velocity is of the order of 10^6, so the inviscid assumption is valid. In order to assume incompressibility, the Mach number squared must be much less than one. This criterion is fulfilled in all regions of the actual ("real life") flow except near the inlet lip where the Mach number is near one; however, compressibility effects are still considered to be insignificant in the examination of this phenomenon since the locally high Mach number would be expected to have little influence on the overall phenomenon.

Since both the actual flow and the investigated flow possess the above specifications, it is valid to use the experimental results to infer information about the actual flow. In addition, the details of the mechanisms producing the inflow should not be critical to the process of vortex formation; therefore, it is justifiable to carry out the

investigation independent of the turbomachinery components.

3.2 VORTICITY PRINCIPLES

Vorticity, $\underline{\omega}$, is proportional to the local angular velocity of a fluid particle, and it is related to the velocity by the following equation:

$$\underline{\omega} = \nabla \times \underline{V} \tag{1}$$

where $\underline{V}$ is the velocity. A convenient method of describing the vorticity in a flow field is to analyze the motion of the vortex lines associated with the vorticity. Feynman (2) defined vortex lines as mean field lines that have the direction of $\underline{\omega}$ and a density proportional to the magnitude of $\underline{\omega}$ in any region. The assumptions stated in the previous section further simplify the study of vorticity and its amplification. For these constraints the circulation for every contour enclosing a vortex line remains constant; the vortex lines must therefore either form closed loops or end at a fluid boundary. They can never be cut or end in the fluid. In addition, a fluid line or material line that at any instant coincides with a vortex line will do so forever and the ratio of the vorticity to the length of the line remains invariant in time for a material line. Consequently, the elongation of a material line implies stretching of a vortex line which denotes an increase in vorticity. These vortex principles are known as Helmholtz's laws and are described in detail by Shapiro in reference (3).

3.3 THE INVESTIGATED FLOW

In this investigation, the ambient vorticity typically present in the vicinity of an outdoor engine test stand and airfield, i.e. the wind shear,is simulated in the water tunnel by using non-uniform honeycomb to create several shear profiles. The profile can have either vertical or horizontal components of vorticity. Normally, the vorticity found in wind shear is small in magnitude; therefore, it must be substantially amplified in the region of the engine for an inlet vortex to form. It is the objective of this study to obtain the three dimensional inlet flow field and the vortex formation mechanisms by determining the variation of this vorticity between a far upstream location and the engine inlet. Since material lines are vortex lines, the amplification or reduction of the vorticity is discerned by marking a material line with hydrogen bubbles and observing its path and deformation as it is convected downstream and ingested into the inlet. The path followed by the material lines gives insight into the inlet velocity field, and its deformation indicates the strength of the vortex since the magnitude of the vorticity is directly proportional to the length of the vortex line. The mechanisms of formation are deduced by comparing the above observations.

To determine the necessity of ambient vorticity in the formation of an inlet vortex, irrotational flow was investigated. In this case, there is no ambient vorticity present and there are no upstream vortex lines. However material

lines (time lines) can still be used to study the flow field around and inside the inlet.

CHAPTER 4

EXPERIMENTAL APPARATUS

4.1 WATER TUNNEL CONFIGURATIONS

4.1.1 G.T. & P.D.L. Small Water Channel

The M.I.T. Ocean Engineering Water Tunnel was used to carry out the main part of this experimental investigation. However, this facility is in high demand so a smaller water channel was first constructed to facilitate the development of an appropriate flow visualization technique and shear profile generator. The principal design objectives of this small channel were the delivery of irrotational laminar flow at velocities up to 0.15 m/sec and a minimal construction time. This latter requirement was particularly responsible for the unorthodox design shown in Figure 3. The 3.2 mm hexagonal cell honeycomb, the 80 pores per inch polyurethane foam and the 33, 6.4 mm diameter, holes per linear inch stainless steel screen were all necessary to straighten the flow and suppress turbulence. Kraft paper treated with plastic was used for the honeycomb. The channel was constructed using 19 mm plexiglass and the piping is all Gauge 40 Polyvinyl Chloride (PVC). The flow in the channel is driven by a one and a half horsepower centrifugal pump and measured by a vertical flowmeter. More detailed information about the equipment can be found in Appendix 1.

It should be mentioned that prior to using honeycomb,

the ability of stainless steel mesh screens, perforated plates, porous foam and straws to produce shear flows was investigated in the small channel. They were all found to be unsuitable, because they either failed to create the appropriate shear or induced turbulence and local flow non-uniformities in the downstream flow.

4.1.2 M.I.T. Ocean Engineering Water Tunnel

All of the flow visualization studies were carried out in the 6,000 gallon capacity M.I.T. Ocean Engineering Water Tunnel. A schematic of this facility is shown in Figure 4. The 1.5 m long, 0.5 m square test section is equipped with four interchangeable 0.038 m thick plexiglass windows. In this investigation, it was run with a free surface. The test section is preceeded by a settling chamber and a contraction to reduce velocity non-uniformities and turbulence level in the tunnel. A honeycomb structure fabricated from 1,944 acrylic tubes each with a diameter of 0.03 m and a length of 0.30 m is contained in the settling chamber. This structure is followed by three wire screens with 0.43 m diameter wires spaced 3.18 mm apart. The contraction section is made out of fiberglass reinforced plastic and stiffened with a polyurethane foam core. The overall contraction ratio is 4.92:1.

Following the test section, there is a diffuser and a turning vane section; above this vaned section, a vacuum chamber is positioned. The large storage tank on the lower

level of the tunnel permits the draining of the test section; it can be refilled in 3 to 4 minutes using a 350 gallon per minute pump. A 0.77 m I.D. impeller (located at the bottom right corner of the sketch of the tunnel shown in Figure 4) is connected through pulleys to the motor drive; a digital frequency counter connected to this impeller indirectly measures the tunnel velocity. More detailed information can be found in reference (4).

Additional piping was necessary to adapt this facility to the present investigation; however, the pump, rlow meter and flow filter are basically the same units used in the small water channel. A 0.05 m brass gate valve downstream of the flow meter is used to regulate the inlet flow. A 0.08 m plexiglass "false bottom" was also inserted into the test section to facilitate the observance of the vortex between the ground plane and the inlet.

4.2 INLET GEOMETRIES

The engine inlet is modeled in this investigation by a plexiglass pipe, with the suction provded by the centrifugal pump. Three different inlet configurations were studied in some detail: an inlet at zero degrees to the mean flow far upstream; an inlet at ninety degrees to the mean flow far upstream, and

a double inlet configuration at ninety degrees to the mean flow with inside diameters of 0.04 m, 0.05 m and 0.03 m, respectively. All three inlets are (platinum) wired for hydrogen bubble flow visualization to discern the location of the vortex in the inlet. The wire is located 0.03 m downstream of the lip and is situated normal to the inlet axis. The rear of the zero degree inlet was constructed out of plexiglass; therefore, the positioning of a mirror downstream of the inlet enabled the location and the sense of rotation of the vortex in the inlet to be detected. A sketch of the water tunnel test section with a zero degree inlet configuration in a boundary layer type shear is shown in Figure 5.

The ratio of the centerline height from the ground plane or symmetry plane to the inlet diameters was held constant at approximately 1.4 for all three configurations. This is a number typical of the actual centerline height to diameter ratio of several high-bypass gas turbine engines on wide body aircraft.

4.3 GENERATION OF SHEAR PROFILES

The generation of artificial shear flows was accomplished by using honeycomb of non-uniform lengths designed according to the calculation procedures developed by Kotansky in (5). A detailed explanation of this method is described in Appendix 2.

Four different shear profiles were created; a boundary layer type flow, a jet type flow, a right to left windshear and a left to right windshear. The first profile was generated from 3.18 mm hexagonal cell honeycomb while the remaining three shear profiles employed 4.76 mm hexagonal cell honeycomb. The velocity profiles can be seen in Figures 6, 7, 8, and 9, respectively. The first two shear profiles have vortex lines that are parallel to the ground plane and normal to the mean flow far upstream. The circulation around material lines associated with the boundary layer type profile is clockwise while that linked to the jet type profile is counterclockwise, when viewed at ninety degrees from the velocity plane. The latter two shear profiles also have vortex lines which are vertical and normal to the mean flow far upstream with the circulation being clockwise and counter-clockwise when viewed looking down on the tunnel. In all four cases, the honeycomb lies on top of the false bottom and is secured to the side walls.

4.4 FLOW VISUALIZATION

Hydrogen bubble flow generation was determined to be the most appropriate flow visualization method for this application. In this investigation, a thin platinum wire was employed as the cathode of a DC circuit used to electrolyze the water. The current travels from the wire through the water to an anode plate far downstream in the tunnel. Hydrogen ions are formed at the cathode. These hydrogen ions

combine to form hydrogen gas which is swept off the wire, by hydrodynamic forces, in the form of hydrogen bubbles. The diameter of these bubbles and their density are proportional to the diameter of the wire and the current, respectively. Since the flow around the bubbles is slow moving and steady, it can be described as a Stokes flow; therefore, a small diameter wire insures that the drag force on the bubbles is greater than the buoyancy force. Consequently, the majority of the hydrogen bubbles follow the flow and are good indicators of the local water velocity. A detailed discussion of this technique is presented in Appendix 3 with information provided by the following references: (6), (7), and (8).

The variable DC power supply was constructed using a variac, a transducer, an AC to DC rectifier and electric circuit elements as described in the above Appendix. It has the capability of delivering up to 300 volts either as a continuous voltage or a pulsed voltage for a wide range of frequencies. Aside from the wires embedded in the inlet, three different wire probes were used to examine the flow: a 0.30 m high vertical probe normal to the upstream mean flow; and a 0.23 m long horizontal probe parallel to the ground plane and normal to the upstream flow and a smaller probe which could be inserted at various positions in the flow field. They all used 0.025 mm wire. Since the inlet velocity was much higher than the tunnel velocity, the wires used in the inlet were thicker and the bubbles consequently

larger. However, no evidence was seen of any important effects of buoyancy. The struts supporting the wires were formed from plexiglass and plastic. For the first two probes, they were streamlined to minimize their disturbance to the surrounding flow field.

The proper illumination of hydrogen bubbles is critical in observing and photographing them. In this experiment, suitable lighting was achieved by using two 0.28 m square Fresnel lens, with 0.24 m focal length and a tungsten halogen lamp. The two lenses were situated parallel to each other with the first lens directly above the area to be illuminated and the second lens a few centimeters above it. The lamp was located a focal length above the second lens.

The hydrogen bubble data was photographed and videotaped. The instamatic photographs were taken using a Calumet 4 x 5 View Camera using Polaroid Type 57 film. The videotaped data required a videocamera, a videorecorder, a videoprojector, and a power source.

CHAPTER 5

EXPERIMENTAL PROCEDURE

Prior to starting the flow visualization study, the M.I.T. Ocean Engineering Water Tunnel was deaerated for several hours. Then the tunnel velocity and the inlet velocity were set to the desired reading. Since each honeycomb shape had a different resistance, the velocity was calibrated separately for each screen. This was accomplished by taking photographs of streamlines pulsed at a selected frequency for a wide range of tunnel frequency counter readings. Photographing a known length relates the image distance to the acutal distance by a constant; therefore, the velocity can easily be deduced from the photographs since the time is given by the pulsing rate.

The flow around the single inlet was investigated with all three probes for each of the four shear profiles at zero degrees and ninety degrees of yaw. In addition to the above two orientations, the single inlet and double inlet in irrotational flow were also studied at two hundred and seventy degrees of yaw. The transient conditions involved in the inlet vortex start up and cessation, for the single inlet and double inlet configurations oriented at ninety degrees to the mean upstream flow, were examined by decreasing the tunnel velocity while keeping the pump velocity constant at 1.2 m/sec and by keeping the tunnel speed constant at 0.08 m/sec and decreasing the pump setting until the vortex disappeared.

CHAPTER 6

EXPERIMENTAL OBSERVATIONS

As stated, flow visualization experiments were conducted with several inlet-ambient flow combinations. In this section, we will describe the experimental observations. The next section will then present a discussion and interpretation of these observations. It should be noted that this investigation was not a parametric study; the objective was to create a vortex typical of those actually observed at a centerline height to diameter ratio of approximately 1.4 and to determine the important features of the flow and the vortex generating mechanisms.

The tests included both steady flow and (start-up and stop) transient studies with an inlet-ground plane configuration, similar to the physical geometry of the actual situation, as well as with a double inlet configuration which was located in the center of the water tunnel far from the ground plane. In this latter case, there was a plane of symmetry between the inlets (i.e. one inlet could be viewed as the "image" of the other) so that we essentially had a boundary layer free analogue of the ground plane. This enabled us to investigate inlet vortex formation with (nominally) no ambient vorticity upstream of the inlet. The double inlet studies were conducted with irrotational flow only; however, the single inlet studies were carried out with a known shear as well as with

irrotational flow. The upstream velocity profiles that were used included cases with horizontal vortex as well as vertical vortex lines.

The overall matrix of experiments that were conducted was as follows:

Single Inlet:

Yaw	Flow	Time Dependence
zero degrees	irrotational flow	steady
	horizontal vortex lines (boundary layer)	steady
	horizontal vortex lines (jet)	steady
	vertical vortex lines (clockwise*)	steady
	vertical vortex lines (counterclockwise*)	steady
ninety degrees	irrotational flow	steady & transient
	horizontal vortex lines (boundary layer)	steady
	horizontal vortex lines (jet)	steady
	vertical vortex lines (clockwise*)	steady
	vertical vortex lines (counterclockwise*)	steady
two hundred and seventy degrees	irrotational flow	steady

Double Inlet:

ninety degrees	irrotational flow	steady & transient
two hundred and seventy degrees	irrotational flow	steady

*As observed looking down on the tunnel

Although it may seem to be in reverse order, we will describe the results with the shear first since the mechanism of vortex formation is most readily understood within the background of the theoretical calculations reported in previous M.I.T. Gas Turbine Lab studies. We will then describe the results with irrotational flow, because it is in this situation that the new mechanism was made apparent. The results with the double inlet will then be mentioned, since they are helpful in understanding this new mechanism of inlet vortex formation.

6.1 SINGLE INLET IN SHEAR FLOW AT ZERO DEGREES OF YAW

6.1.1 Boundary Layer Type Profile

In this case and the other cases with a known shear flow, the ingestion of ambient vorticity can be directly studied since (outside of the viscous vortex core or the (thin) ground plane and inlet boundary layers) vortex lines are material lines. A line of hydrogen bubbles is to a very good approximation a material line; the hydrogen bubble lines also give the position of vortex lines as they are convected into the inlet. One is therefore able to speak with a reasonable degree of confidence about the kinematics of the vortex lines associated with the ambient vorticity.

A vortex filament in a ground plane boundary layer type velocity profile is initially horizontal, parallel to the ground plane, perpendicular to the mean flow, and possess clockwise rotation when viewed at ninety degrees from the

velocity profile plane. Its ingestion by an inlet at zero degrees to the mean flow is illustrated in Figure 10. This sketch, of the actual phenomenon as indicated by the hydrogen bubble marked material lines, displays the symmetrical pattern formed by the vortex lines about the vertical centerline of the inlet; the central portion of this line is ingested prior to the two "ends" which enter the inlet for the line chosen at roughly 0.9 inlet centerline heights. Photographs of this behavior for three successive time intervals are presented in Figure 11a, 11b, and 11c, respectively,with the initial inlet flow influence occuring at approximately one centerline height upstream of the inlet.Figure 12 is a view of the above flow as observed in a mirror located downstream of the inlet for a vortex originating at roughly 0.9 inlet centerline heights. The position of a vortex in the inlet will be described by referring to the inlet area perpendicular to the flow in terms of a clock face. Thus, using this nomenclature, the vortices visible in Figure 12 are located at 5:30 and 6:30; the rotation exhibited by the two vortices appears equal and opposite with the former turning clockwise and the latter counterclockwise when viewed looking into the inlet. At the capture area investigated (~8), this behavior is true for vortex lines approximately 0.5 inlet centerline heights or lower. If they originate at a greater height, they proceed straight into the inlet without any rotation.

The investigated capture area was selected by examining the inlet vortex over a wide range of capture areas and

selecting one that resulted in a strong steady vortex for configurations typical of current wide body aircraft, i.e. H/D ~ 1.4. This vortex is typical of those observed under genuine operating conditions; therefore, an understanding of the salient features of the flow and of the mechanisms generating the vortex can be obtained by studying this reproduction of the actual phenomenon.

6.1.2 Jet Type Profile

The jet profile consisted of a strong shear layer. It required substantially higher inlet velocities, i.e. larger capture areas for a vortex to form than with the boundary layer type profile. Consequently, the usefulness of the flow visualization probes was limited, and only a small amount of data was obtained.

Vortex lines associated with the jet type flow and boundary layer type flow are both horizontal, but the circulation around a vortex line linked to the former is counter-clockwise when viewed at ninety degrees from the velocity profile plane. Since the vorticity present in the geometrically-symmetric zero degree inlet configuration is equal and opposite, the convection downstream and ingestion of these vortex lines should be equivalent; this inlet configuration was therefore not examined for the jet type profile.

In actuality, a thin ground plane boundary layer also existed with the jet shear. However, its height was negligible

relative to the thickness of the shear layer.

6.1.3 'Right to Left' Windshear

In this case, the vortex lines associated with the shear are initially vertical, perpendicular to the ground plane, normal to the mean flow and possess a clockwise rotation when viewed looking down on the tunnel. Figure 13 denotes the vortex inlet location for the zero degree inlet configuration as observed through a mirror downstream of the inlet. It indicates that a single steady clockwise rotating vortex is present in the inlet at approximately 6:00 and at 0.8 inlet centerline heights. The vortex leg directly in front of the inlet reveals when looking down on the tunnel a large clockwise spiraling vortex extending between the ground plane and the inlet with the diameter of the spiral diminishing as it moves toward the inlet; a photograph of this flow is shown in Figure 14. In the center of the spiral, a hydrogen bubble marked thread of fluid particles moves vertically up and into the inlet. This observation is in agreement with the calculations of Viguier (1) who found that the lower legs of initially vertical vortex lines which were perpendicular to the mean flow are squeezed around the forward stagnation streamline forming a localized area with a high vorticity distribution, i.e. an inlet vortex. Viguier also concluded that the upper legs of these vortex lines "fanned out" over the upper part of the inlet; however, observations of this latter effect was beyond the capability of the existing experimental program.

Further investigation of the flow indicated that at the capture areas studied, the inlet's influence was felt roughly 2.5 inlet centerline heights above the ground plane, 1.5 inlet centerline heights to either side of the vertical centerline, and approximately 1 inlet centerline height in front of the inlet face. In this examination, the inlet was situated directly in the center of the tunnel; however, shifting the inlet's position while keeping its allignment constant did not produce any distinguishable deviation in the vortex position or rotation.

6.1.4 'Left to Right' Windshear

Although the circulation around the vertical vortex lines associated with this shear profile was counterclockwise, when viewed from the top of the tunnel, the features detected for the zero degree inlet configuration were very similar to those observed in the previous case with clockwise circulation, except of course for the sense of the vortex rotation. Both profiles possessed a single strong vortex at the same inlet position and centerline height. However, the rotation perceived in this case was counterclockwise looking into the inlet.

6.2 SINGLE INLET IN SHEAR FLOW WITH NINETY DEGREES OF YAW

6.2.1 Boundary Layer Type Flow

Some of the features described for a boundary layer type flow drawn into an inlet at zero degrees to the mean upstream flow are also observed for the ingestion of the same type of

flow into an inlet oriented at ninety degrees to the upstream flow, as depicted in Figure 15 for a horizontal vortex line originating at roughly 0.9 inlet centerline heights above the ground plane. Namely a central section is again drawn into the inlet first with the two "ends" entering at a later time, and the vortices enter the inlet at the same height and position with a consistent sense of rotation. However, the flow pattern is asymmetrical and the two vortices do not appear to be equal in strength. The clockwise vortex as viewed looking into the inlet encompasses a larger proportion of the inlet area and appreas to rotate faster; this clockwise leg of the vortex line also swings out in front of the inlet prior to being ingested while the counterclockwise leg follows the outside contour of the cylinder until it is drawn into the inlet. As vortex lines of different heights are examined, additional insight concerning the flow beneath and in front of the inlet can be discerned. Figure 16 illustrates the path taken by a horizontal vortex line initially at 0.1 inlet heights above the ground plane. The counterclockwise leg appears to stem from the separation region located underneath the inlet and 0.8 to 0.9 inlet centerline heights from the inlet lip. It remains at the same height and moves horizontally towards the inlet lip where it is drawn vertically up and into the inlet at the 6:30 location. Simultaneously, the clockwise vortex leg reveals a large clockwise spiraling flow extending between the ground plane

and the inlet in the region directly in front on the right half of the inlet with the spiral's diameter decreasing as it approaches the inlet. A hydrogen bubble marked thread of fluid particles extends vertically up through the center of the spiral and into the inlet. Outside of the inlet, the clockwise spiral encircles the counterclockwise vortex leg; consequently, it is difficult to perceive both legs concurrently. If the vortex line is initially greater than or equal to 0.6 inlet centerline heights above the ground plane for the capture area investigated (~8) the clockwise leg is ingested without being caught up in the outside spiral.

6.2.2 Jet Type Profile

For the ninety degree inlet configuration, the ingestion of an initially horizontal vortex line possessing counterclockwise circulation results in the formation of a clockwise rotating vortex as viewed looking into the inlet. It was observed at approximately 6:00 and 0.7 inlet centerline heights above the ground plane. As explained previously, only limited data was taken for this case, and no additional observations could be made.

6.2.3 'Right to Left' Windshear

Changing the inlet orientation from zero to ninety degrees with the mean flow for this shear profile did not alter the position or rotation of the vortex in the inlet; therefore, the observations for both inlet orientations were quite similar.

6.2.4 'Left to Right' Windshear

When the ninety degree inlet configuration was investigated in a shear profile with vertical vortex lines possessing counterclockwise rotation when viewed looking down on the tunnel, a clockwise rotating vortex was observed looking into the inlet as shown in Figure 17, at approximately 6:00 in the inlet at a height above the ground plane of roughly 0.7 centerline heights.

6.3 SINGLE INLET IN IRROTATIONAL FLOW

The presence of the clockwise rotation bias exhibited in the ninety degree inlet configuration motivated investigating the inlets in an irrotational flow. If the flow is irrotational there is no ambient vorticity present. Consequently, there are no upstream vortex lines and the investigation is confined to studying the flow field around and inside the inlet.

6.3.1 Single Inlet in Irrotational Flow at Zero Degrees of Yaw

For an inlet at zero degrees to mean uniform upstream flow, two small equal symmetric and counterrotating vortices are observed looking into the inlet. This showed that any ambient vertical vorticity in the tunnel was quite small.

6.3.2 Single Inlet in Steady Irrotational Flow at Ninety Degrees of Yaw

A strong steady inlet vortex at 6:00 was observed for an inlet oriented at ninety degrees to the mean flow with a clockwise rotation sense when viewed looking into the inlet. Further investigation of this configuration revealed a

previously undetected feature of the flow field surrounding the inlet. There is a trailing vortex shed from the downstream side of the inlet as illustrated in Figure 18. Relative to the small and concentrated inlet vortex, the trailing vortex is much larger with a swirl diameter of approximately 0.9 inlet diameters and exhibits a clockwise rotation when viewed from the upstream section of the tunnel. The vortex lines and the material lines associated with this flow are depicted in Figures 19 and 20, respectively. This trailing vorticity was connected to a movement in the separation point of the flow from the inlet's surface which varied along the length of the inlet as illustrated in Figure 21. In the rear of the inlet, i.e. far from the lip along the inlet axis, the flow separated at approximately 12:00 and 6:00 from the inlet. This roughly symmetric separation implies nearly zero circulation which is the expected result for a two-dimensional flow over a cylinder and near a ground plane at the present H/D value.(9) Proceeding along the inlet axis towards the inlet lip revealed the development of assymetric flow separation. In addition, the velocities appeared to be substantially higher than in the rear and both of these conditions indicate a significant circulation round the inlet near the lip. At this location, the hydrogen bubbles show the flow separation occurring at 4:00 and 6:00 as illustrated in the sketch of the streamline for a ninety degree inlet configuration in irrotational flow, Figure 18.

6.3.3 Single Inlet in Steady Irrotational Flow at Two Hundred and Seventy Degrees of Yaw

To check for the presence of ambient vorticity, an inlet oriented at two hundred and seventy degrees to the mean flow was used to investigate the irrotational flow. It possessed a steady strong vortex at approximately 6:00 which exhibited counterclockwise rotation when viewed looking into the inlet.

6.3.4 Single Inlet in Transient Irrotational Flow at Ninety Degrees of Yaw

Presumably, the asymmetric separation of the flow is due to an interaction between the ground plane and the inlet lip which causes the initially two-dimensional flow over the inlet to become inherently three-dimensional. To understand the development of this feature, the inlet vortex and trailing vortex formation are examined during the transient response of the ninety degree inlet in irrotational flow. Initially, the tunnel velocity was very high; therefore, the stagnation point on the ground was blown away. Consequently, a vortex did not form and the flow symmetrically separated from the inlet lip at roughly 3:00. Holding the inlet velocity constant and decreasing the tunnel speed resulted in the flow separation points shifting to 4:00 and 6:00. The separation point moved in a clockwise direction along the inlet suface and gave rise to a trailing vortex which propagated downstream. Figures 22a to 22d photographically represent this successive shifting in position of the separation point at the inlet lip during

the transient response. The flow beneath the inlet cannot be seen in the above figures due to the difficulty in simultaneously lighting the regions above and below the inlet; however, the inlet vortex position is revealed by the inlet flow visualization wires and is shown in Figure 23.

The transient response of the system therefore displayed the movement of the inlet lip's separation point as well as the formation of the inlet vortex and the trailing vortex. These three features are all interrelated and are regulated by the tunnel velocity to inlet velocity ratio, U_∞/U_i. For high U_∞/U_i, there were no vortices but as this velocity ratio decreased the vortices appeared and became stronger.

6.4 DOUBLE INLET CONFIGURATION IN IRROTATIONAL FLOW

In this arrangement, the ground plane was "replaced" by a symmetry plane between the two inlets with a centerline height to diameter ratio for <u>each</u> of the two inlets of approximately 1.4. The absence of the viscous ground plane boundary layer allows us to study the inlet vortex formation with no ambient vorticity upstream of the inlet.

6.4.1 Double Inlet Configuration in Steady Irrotational Flow at Ninety Degrees of Yaw

The investigation of this flow field revealed a steady strong clockwise rotating vortex core, when viewed looking down on the tunnel, in between the two inlets with a trailing vortex shed from each of the inlets as sketched in Figure 24. Figures 25 and 26 depict the location of the vortex lines, which

when taken as a unit resembles a horseshoe vortex, and the material lines associated with this inlet arrangement, respectively. A photograph of the material lines is shown in Figure 27. The inlet vortex enters the top and bottom inlets at approximately 6:00 and 12:00 with clockwise and counter-clockwise rotation when viewed looking into the inlets, respectively. The center of the core was apparent due to cavitation along its length.

6.4.2 Double Inlet Configuration in Steady Irrotational Flow at Two Hundred and Seventy Degrees of Yaw

As in the single inlet configuration, this orientation was again used to check for the presence of ambient vorticity. The flow examination yielded the same features observed in the previous arrangement, but the sense of rotation of the vortices was again reversed which indicated that the ambient vorticity was at a low enough level so as not to appreciably effect the phenomenon.

6.4.3 Double Inlet Configuration in Transient Irrotational Flow at Ninety Degrees of Yaw

A fundamental question still remains unanswered for the (inviscid) double inlet orientation. Namely, where does the vorticity in the core come from? The transient case was investigated in the hope it might resolve this question.

The additional examination showed that the inlet vortex initially formed during the transient process associated with start-up. It originiated in between and slightly downstream

of the two inlets; therefore, it is initially fed by the fluid in that region. As the vortex formed and became stable it moved to the location in front of the inlets illustrated in Figure 28. Once formed, this phenomenon quickly reached equilibrium and was no longer fed by the downstream flow; however, there is a time delay on the order of ten convection time scales (i.e. $O(10H/U_\infty)$) associated with its formation. When the inlet flow is arrested, the vortex detached from the inlets and burst into the region immediately downstream of the inlet.

CHAPTER 7

DISCUSSION OF RESULTS

The central results of the flow visualization studies are summarized in Table 1. Although this table cannot include all the information about the various cases, it will provide a convenient framework from which to discuss them. As in the previous section, we will discuss the results with ambient shear first, and then compare these with the theoretical calculations of Viguier.

7.1 SINGLE INLET IN SHEAR FLOW AT ZERO DEGREES OF YAW

7.1.1 Boundary Layer Type Profile

As noted previously, a horizontal vortex line initially exhibiting clockwise rotation gave rise to two symmetrically located counterrotating vortices when ingested into an inlet oriented at zero degrees to the far upstream flow. This is readily understood from considerations of flow symmetry and solenoidality of the vorticity field and will not be further discussed except to note that it gives a good indication of the overall symmetry of the tunnel flow.

7.1.2 'Right to Left' Windshear

The behavior of vertical vortex lines ingested into an inlet at zero degrees to the far upstream flow was computed by Viguier in reference (1), and his method is summarized in the background section of this report. Since vortex lines cannot be cut, the ingestion of a central section of a vortex

line indicates that two vortex legs must extend out of the inlet. Viguier found that the upper legs of the vortex lines were "fanned out" over the upper part of the inlet while the lower legs were squeezed around the forward stagnation point. This implies a locally high level of circulation per unit area in the latter region which strongly suggests the formation of an inlet vortex. As denoted in Table 1, the experimental result for a zero degree oriented inlet ingesting a vertical vortex line exhibiting clockwise rotation when viewed looking down on the tunnel is in agreement with Viguier's for the lower legs. The vertical vortex lines are convected downstream and, due to the flow field associated with the inlet, result in a centralized vorticity distribution at the engine face possessing the same rotation sense. The "fanning out" of the upper region of the vortex leg could not be observed within the constraints of the present experimental program. This amplification of the upstream ambient vorticity as the vertical vortex lines are stretched at the inlet face is one basic method of vortex formation.

7.1.3 'Left to Right' Windshear

As in the previous case, the ingestion into a zero degree oriented inlet of the vertical vortex lines associated with this profile produced an inlet vortex exhibiting the same sense of rotation as the vortex lines, i.e. the rotation was reversed from case 7.1.2. This result therefore also supports Viguier's conclusion and gives added justification to con-

sidering the amplification of the upstream ambient vertical vorticity as one mechanism of vortex formation.

7.2 SINGLE INLET IN SHEAR FLOW WITH NINETY DEGREES OF YAW

7.2.1 Boundary Layer Type Flow

Based on Viguier's calculations, it was expected that the ingestion of horizontal vortex lines into a ninety degree oriented inlet would result in two asymmetrically placed counterrotating vortices so that in contrast to 7.1.2 and 7.1.3 no predominant single concentration of vorticity was predicted. Within the context of this secondary flow anslysis, the circulation around the two legs will be of the same magnitude, but the vorticity is not necessarily equal. The vortices observed were in fact not equal in strength; the clockwise vortex encompassed a larger area and had a faster rotation rate and the overall flow field outside the inlet was dominated by this vortex. Consequently, the qualitative picture provided by Viguier does not fully describe the flow. One might thus expect that another phenomenon must be occurring other than just the stretching of ambient far field vorticity; this will, in fact, be seen to be the case.

7.2.2 Jet Type Profile

The investigation of horizontal vortex lines initially possessing counterclockwise rotation revealed a single strong clockwise rotating vortex as viewed looking into the inlet. Possibly, the second vortex is hard to find; however, if the only mechanism was the amplification of ambient vorticity

the stronger vortex should exhibit a counterclockwise rotation. This is therefore an indication that a clockwise bias is associated with this phenomenon when the inlet is oriented at ninety degrees to the far upstream flow.

7.2.3 'Right to Left" Windshear

For an inlet oriented at ninety degrees to the mean upstream flow, the ingestion of vertical vortex lines initially exhibiting clockwise rotation when viewed looking down on the tunnel gave rise to a single clockwise vortex inside the inlet. This observation was expected, and the rationale discussed in the section dealing with the ingestion of identical vortex lines into a zero degree inlet configuration.

7.2.4 'Left to Right' Windshear

Suprisingly, the ingestion of vertical vortex lines exhibiting counterclockwise rotation when viewed looking down on the tunnel resulted in the formation of a single clockwise rotating vortex inside the inlet. As in the preceeding case, it was anticiapted that only a single vortex would form; however, its sense of rotation was expected to be consistent with the rotation inititally exhibited by the entering vortex line, i.e. counterclockwise. This is therefore a third indication of a clockwise rotation tendency for an inlet positioned at ninety degrees to the upstream flow.

7.3 SINGLE INLET IN IRROTATIONAL FLOW

The clockwise rotational bias exposed in the investigation of the ninety degree inlet configuration prompted the

examination of the inlet flow field with initially uniform flow far upstream, i.e. channel flow with no added resistances. This irrotational flow study was undertaken to see whether the clockwise inclination was created by either some bias in the tunnel flow or if a fundamentally new mechanism of vortex formation is present. If the tunnel flow is inherently non-uniform, the inlets will act as amplifiers of this vorticity and the vortex rotation should consistently have the same sense. However if vortices are present and exhibit different directions of vortex rotation for different inlet orientations, a new method of vortex generation is indicated.

7.3.1 Single Inlet at Zero Degrees of Yaw

When the zero degree inlet was used, we found two equal and opposite vortices inside the inlet, thus denoting the absence of any appreciable vertical vorticity.

7.3.2 Single Inlet at Ninety Degrees of Yaw

A strong steady clockwise vortex was observed when viewed looking into the tunnel. This indicates the presence of vorticity in the flow at least in the vortex core; however, no conclusions concerning the cause of this vortex can be formulated without additional information.

7.3.3 Single Inlet at Two Hundred and Seventy Degrees of Yaw

The investigation of this inlet configuration revealed a single counterclockwise rotating vortex when observed looking into the inlet. This observation in conjunction with the preceeding one rules out the possibility of the vortices being

due to ambient vertical vorticity if the vortices in the case and the prior case both exhibited clockwise rotation when viewed looking into the inlet, it would indicate a non-uniform tunnel velocity field. However, the above vortices exhibit opposite rotation. The tunnel velocity is therefore essentially irrotational and a mechanism other than the amplification of ambient vorticity must be responsible for the vortex generation.

7.3.4 Re-examination of Single Inlet at Ninety Degrees of Yaw

A further investigation of the flow for this configuration revealed the presence of a trailing vortex downstream of the inlet in addition to the inlet vortex. This should in fact be expected since far from the inlet lip there is nothing in the flow to create the torque needed to cause appreciable circulation round the inlet. At this far field location, the flow can therefore be approximated by two dimensional flow about a cylinder-ground plane configuration with the cylinder axis positioned perpendicular to the free stream velocity. In this case as described in Bearman (9), the circulation around the cylinder is quite small at the H/D investigated; therefore, the circulation around the inlet at any axial location far from the inlet is near zero. However, if only a single vortex was associated with the inlet, a large (net) circulation would exist at any axial station along the length of the inlet. This condition is thus incompatible with the preceeding description of the flow around the inlet in the

far field; consequently, an inlet with only a single vortex is not possible. The circulation must therefore increase as one examines stations closer to the lip, and this change in circulation will result in vortex lines trailing downstream. An analogous though converse example of circulation changing with axial position is the finite wing porblem. In this case the circulation has a net value around the tip of the wing and is approximately zero on the body.

This change in circulation could be observed using the flow visualization technique to examine the separation points of the flow from the inlet surface. A symmetric separation and streamline pattern indicates essentially zero circulation as sketched in Figure 21. The observed circulation was close to zero at axial distances over a diameter from the inlet lip, and a pronounced clockwise circulation was evident at the inlet lip as illustrated in Figures 22a and 22d, respectively. Presumably, the asymmetric flow separation, i.e. the clockwise circulation,is due to the non-symmetrical pressure field resulting from the ground plane and cylinder interaction when there is a large ratio of inlet to far upstream velocity. However, whatever the detailed mechanism, it is clear that the variation of circulation with axial distance along the inlet length is directly linked to the generation of the trailing vortex system, and is therefore a new method of vortex formation.

7.3.5 Single Inlet in Transient Irrotational Flow at Ninety Degrees of Yaw

In order to obtain further insight into the overall mechanism, it was suggested by Marble (10) that the transients, i.e. starting or stopping of the pump be investigated. The response of the ninety degree inlet configuration in irrotational flow to a transient variation in U_∞/U_i displayed the movement for the separation point at the inlet lip and the formation of the trailing vortex system. For high values of U_∞/U_i, there were no vortices inside the inlet; however, vortices appeared and intensified as this velocity ratio was decreased. Consequently, the value of this ratio is a key parameter in determining the three dimensional flow at the inlet lip and therefore the circulation. At high values of U_∞/U_i, the flow at the inlet lip does not "feel" the presence of the ground, i.e. the captured streamlines do not hit the ground. The flow around the inlet is therefore symmetrical, and the circulation is essentially zero. Consequently, no vortices form. However as U_∞/U_i is decreased, an interaction between the ground plane and the inlet must occur which results in an asymmetric pressure field and thus a non-symmetric flow separation at the inlet lip.

7.4 DOUBLE INLET CONFIGURATION IN IRROTATIONAL FLOW

Once the inlet vortex in the preceeding cases is formed, it is fed by the ground plane boundary layer. The major part of the flow field, however, does not seem to be significantly

influenced by any viscous effects. In order to investigate the dependence of the vortex formation on the existence of a viscous boundary layer, the double inlet configuration was examined.

7.4.1 Double Inlet Configuration in Steady Irrotational Flow at Ninety Degrees of Yaw

The presence of the trailing vortex system shown in Figures 24 to 27 for this essentially vorticity free upstream flow indicates that neither the ground plane not ambient vorticity are essential for vortex formation. In addition, from observations of the hydrogen bubbles, the circulation around the inlet can again be seen to vary with axial distance from the inlet lip. It was also noted that the vortex core stretched between the two inlets; but there was no feeding of the vortex from fluid downstream of its tunnel position.

7.4.2 Double Inlet Configuration in Steady Irrotational Flow at Two Hundred and Seventy Degrees of Yaw

This orientation was used as an additional check on the presence of ambient vorticity in the tunnel. Since the trailing vortex system with a reversed sense of rotation was observed, it indicates the relative absence of ambient vorticity in the flow.

7.4.3 Double Inlet Configuration in Transient Irrotational Flow at Ninety Degrees of Yaw

In order to better understand this new mechanism and to determine the source of the vorticity present in the core, the

double inlet configuration is investigated while undergoing a transient response. It revealed that the vortex was formed during the transient start-up process and that it reached equilibrium in a time on the order of ten H/U_∞ . Since there is no ambient vorticity and no boundary layer, the transient process must produce a source of vorticity. However, vorticity can only be generated by viscosity and the only viscous fluid present in this configuration is contained in the boundary layer on the inlet's surface. Therefore, the vorticity must come from the surface of the inlets during the start-up process, and in fact the flow visualization shows the vortex core starting immediately downstream of the inlets and moving to a position between the inlets once a stable core is formed. The time delay in forming the vortex is probably due to the time required for the inlet surface boundary layer and its associated vorticity to be shed into the main flow. Once formed, the vortex core is maintained by vortex straining with the vorticity produced by vortex stretching balancing the diffusion; consequently, the phenomenon exists in dynamic equilibrium as deduced by Marble (10).

This examination proved that ambient vorticity was <u>not</u> necessary for the formation of an inlet vortex and that the variation in circulation along the axial length of the inlet was indeed capable of generating a vortex for an inlet in crosswind, i.e. at ninety degrees to mean upstream flow.

CHAPTER 8

CONCLUSIONS

Two basic mechanisms of inlet vortex formation have been found. The first is associated with the production of a vortex in a flow possessing ambient vertical vorticity. It is the amplification of this ambient vorticity as the vertical vortex lines are stretched and drawn into the inlet that is responsible for the formation of an inlet vortex. However, ambient vorticity is not essential for the generation of a vortex. In the second mechanism, an inlet vortex is created with an inlet in crosswind in an irrotational flow. Associated with the vortex is a variation in circulation along the axial length of the inlet and thus a trailing vortex system. The circulation around the inlet at sections far from the lip is therefore quite small.

A relevant parameter in determining the appearance of a vortex is the inlet velocity to upstream velocity ratio. In the first mechanism, it determines the amount of stretching incurred by a vertical vortex line and therefore the vorticity increase. For the second mechanism, this ratio has a strong effect on the separation point from the inlet; consequently, it directly controls the three dimensionality of the flow.

CHAPTER 9

RECOMMENDATIONS

To gain more insight into the inlet vortex phenomenon, additional work is required in the computational analysis as well as in experimental research.

The computational method used to predict the potential flow field must be improved so that it suppresses recirculation and adequately describes the flow at the engine face plane. Recommendations concerning these improvements can be found in Viguier (1).

In addition, the quantification of the vortex formation mechanisms would be very desireable. In rotational flow, this can be achieved by experimentally measuring the circulation during wind tunnel tests. However, deducing the magnitude of the circulation present in the newly discovered mechanism of vortex generation is more complicated and has not yet been resolved. The determination of the mechanism which sets the magnitude of this circulation is thus a crucial part of any further study.

APPENDIX 1

EQUIPMENT INFORMATION

Additional Equipment Information:

1) Gould's Centrifugal Pump, Lunt Moss Co., Mass., Model # 3655, 2 x 2-7, 1750 RPM, 1½ Hp.

2) Vertical Flow Meter, Brooks Instrument Division, Penn., Model # 1114.

3) Flow Filter, Chisholm Corp., R.I., Model # MDY 4463BC4.

4) 20 MHz Function Generator, Waveteck, Mass., Model # 143.

5) Polyvinyl Chloride Gauge 40 Piping, Metropolitan Pipe Inc., Mass.

6) Platinum Wire, Omega Inc. Conn., Order # SPPL-001.

7) Fresnel Lens, Edmund Scientific Co., N.J., 0.28 m square, 0.24 m focal length, St # 72246.

APPENDIX 2

GENERATION OF SHEAR PROFILES

The four artificial shear flows utilized in this investigation were generated using honeycomb of non-uniform lengths designed according to the calculation procedure developed by Kotansky in (5). This method consisted of performing a momentum balance around the honeycomb with the pressure drop across the honeycomb defined as follows:

$$p(o,s) - p_D = \frac{4f(s)L(s)}{D_h} [\tfrac{1}{2}\rho U^2(s)] \qquad (2\text{-}1)$$

where p_D is the pressure downstream of the honeycomb, $p(o,s)$ is pressure just upstream of the honeycomb, f is the friction factor, L is the length of the honeycomb, D_h is the hydraulic diameter of the honeycomb, ρ is the density of the water, U is the velocity, and for a given axial tunnel distance s is the direction in which the velocity profile varies. Upstream of the honeycomb, the flow field is considered to be irrotational with parallel flow at a far upstream location, no flow normal to the walls and a prescribed axial component of velocity at the honeycomb. The flow downstream of the honeycomb is also assumed to be parallel, but it is now rotational with the gradient of the pressure equaling zero. Combining all of the above boundary conditions results in the following equation for the two dimensional stream function, ψ, in the potential flow region upstream of the honeycomb.

$$\psi(x,s) = U_\infty s + \sum_{n=1}^{20} a_n \sin\left(\frac{n\pi s}{\ell}\right) \exp\left(\frac{n\pi s}{\ell}\right) \qquad (2\text{-}2)$$

where

$$a_n = \frac{2}{n\pi} \int_0^{\ell} \cos \frac{n\pi s}{\ell} \, [U(s) - U_\infty] ds \qquad (2\text{-}3)$$

where ℓ is the height of the tunnel, x is the axial direction in the tunnel, and twenty being an amount of Fourier constants capable of adequately describing the flow. The velocity components u and v in the x and s direction, respectively, can be found from:

$$u = \frac{\partial \psi}{\partial s} \qquad v = \frac{\partial \psi}{\partial x} \qquad (2\text{-}4)$$

The substitution of Eq. (2-2) into the equation for v results in:

$$v(o,s) = \sum_{n=1}^{20} a_n \left(\frac{n\pi}{\ell}\right) \sin\left(\frac{n\pi s}{\ell}\right) \qquad (2\text{-}5)$$

where x = 0 corresponds to the axial location of the honeycomb in the tunnel.

In the irrotational flow region ($x \leq 0$), the stagnation pressure is constant along a streamline; hence, Bernoulli's equation between a far upstream location and a location near the upstream honeycomb side can be represented by:

$$p(o,s) - p_\infty = -\tfrac{1}{2}\rho U^2(s) - \tfrac{1}{2}\rho v^2(0,y) + \tfrac{1}{2}\rho U_\infty^2 \qquad (2\text{-}6)$$

Combining Eq. (2-5) and Eq. (2-1) results in obtaining the equation for the honeycomb length, L(s):

$$L(s) = \frac{D_h}{4f(s)} \left[\frac{U_\infty^2}{U^2(s)} + K_o \frac{U_\infty^2}{U^2(s)} - 1 - \frac{v^2(o,s)}{U^2(s)}\right] \quad (2-7)$$

where

$$K_o = \frac{p_\infty - p_D}{\frac{1}{2}\rho U_\infty^2} \quad (2-8)$$

which is a selected parameter. The friction factor, f(s), is determined from

$$f(s) = \frac{16}{Re(s)} \quad (2-9)$$

where

$$Re(s) = \frac{U(s)D_h}{\nu\beta} \quad (2-10)$$

and ν is the kinematic viscosity of water and β is the open area to total area ratio of the honeycomb.

By selecting U(s) and K_o, v(o,s) can be determined from Eq. (2-5) and Eq. (2-3) and f(s) can be obtained from Eq. (2-9) and Eq. (2-10). Thus, the length of the honeycomb is obtainable from Eq. (2-7).

For this experimental set-up, $\beta = 0.77$, $D_h = 0.3$ cm, and $\ell = 0.4$m.

APPENDIX 3

HYDROGEN BUBBLE FLOW VISUALIZATION

3.1 GENERAL DESCRIPTION

There are many different kinds of flow visualization, but hydrogen bubble flow generation was determined to be the most appropriate for this application. It utilizes a fine wire as the cathode in a DC circuit used to electrolyze the water with the second electrode being part of the tunnel or an inserted piece of corrosion resistant metal. Hydrodynamic forces sweep the hydrogen bubbles off the wire and downstream following the path of the flow, and they are made visible by specially arranged lighting. As pointed out by Schraud in (6), this method offers a great deal of flexibility to the experimenter. For instance, probes of different arrangements can be used to illustrate particular characteristics of the flow, or the voltage to the cathode wire can be pulsed creating time lines which provide a qualitative picture of the velocity profile. In addition, hydrogen bubbles do not contaminate flow or require special ducting as dye and other tracing materials do. Many of the other advantages associated with this technique are discussed by Clutter in (7).

3.2 DETAILS OF THE METHOD

Figure 3-1 displays the circuit used in this investigation; it was adapted from the one employed by Clutter in (7). As shown, AC line voltage comes into the circuit and is raised

above ground level by an isolation transformer. A variable resistor in the form of a variac is then used to set the voltage that will eventually appear across the cathode - anode arrangement. The second transformer boosts the AC line voltage to the desired voltage level, and the rectifier transforms the system from an AC voltage source to a DC voltage source. The remaining circuitry establishes the sharp on off voltage characteristics required for good bubble formation. This circuit can either operate as a pulsed voltage source using the pulse generator to power the relay coil or as a continuous voltage source. Sometimes wires that were operating satisfactorily suddenly begin to function sporadically. Clutter(7) recommended inverting the polarity across the wire for a few minutes when this occurs; therefore, a polarity reversing switch was put into the circuit.

As mentioned previously, a fine wire is used as the cathode in the circuit. Many different types of materials have been used very effectively for hydrogen bubble generation, but we chose to use platinum because it does not corrode and it has been reported to accumulate dirt less rapidly than other materials.The fine diameter wire is used to minimize flow disturbances and to keep the size of the bubbles small. Mattingly in (8) suggested keeping the Reynolds number, dependent on wire diameter,at a value less than fourty to avoid shedding vortices from the wire and therefore flow disturbances. The size of the bubbles produced by the wire

is proportional to the wire diameter; hence, it is also necessary to use a thin wire since only small diameter bubbles follow the actual path of the local velocity field. A gas bubble moving at a slow steady speed can be approximated by Stokes Flow with the forces in the flow described by:

$$\frac{\text{Buoyancy Force}}{\text{Drag Force}} = gd^2/18\nu U(s) \qquad (3\text{-}1)$$

where g is the gravity. It is apparent from the above equation that if the diameter is small, the drag force predominates and the bubble path will accurately exhibit the flow path. To maintain good bubble quality, it is also advisable to keep the wire voltage uniform, and this was achieved in the experiment by connecting two leads to the wire whenever possible.

The circuit utilized is capable of delivering up to three hundred volts; however, one hundred volts was the maximum amount required during the experimentation.

Table 1

SINGLE INLET RESULTS			
Velocity Profiles	Initial Direction of Vortex Lines	Orientation of Inlet to the Mean Flow	Direction of Vortex - Viewed Looking into the Inlet
Vertical Shear Layer (Horizontal Vortex Lines)	CW*	0^o	CW equal CCW
		90^o	CW (stronger) CCW
	CCW*	0^o	not invest.
		90^o	CW
Horizontal Shear Layer (Vertical Vortex Lines)	CW**	0^o	CW
		90^o	CW
	CCW**	0^o	CCW
		90^o	CW
Irrotational Flow	No Ambient Vorticity	0^o	None
		90^o	CW
		270^o	CCW

* Looking at Ninety Degrees to the Plane of the Velocity Profile

** Looking Down on the Tunnel

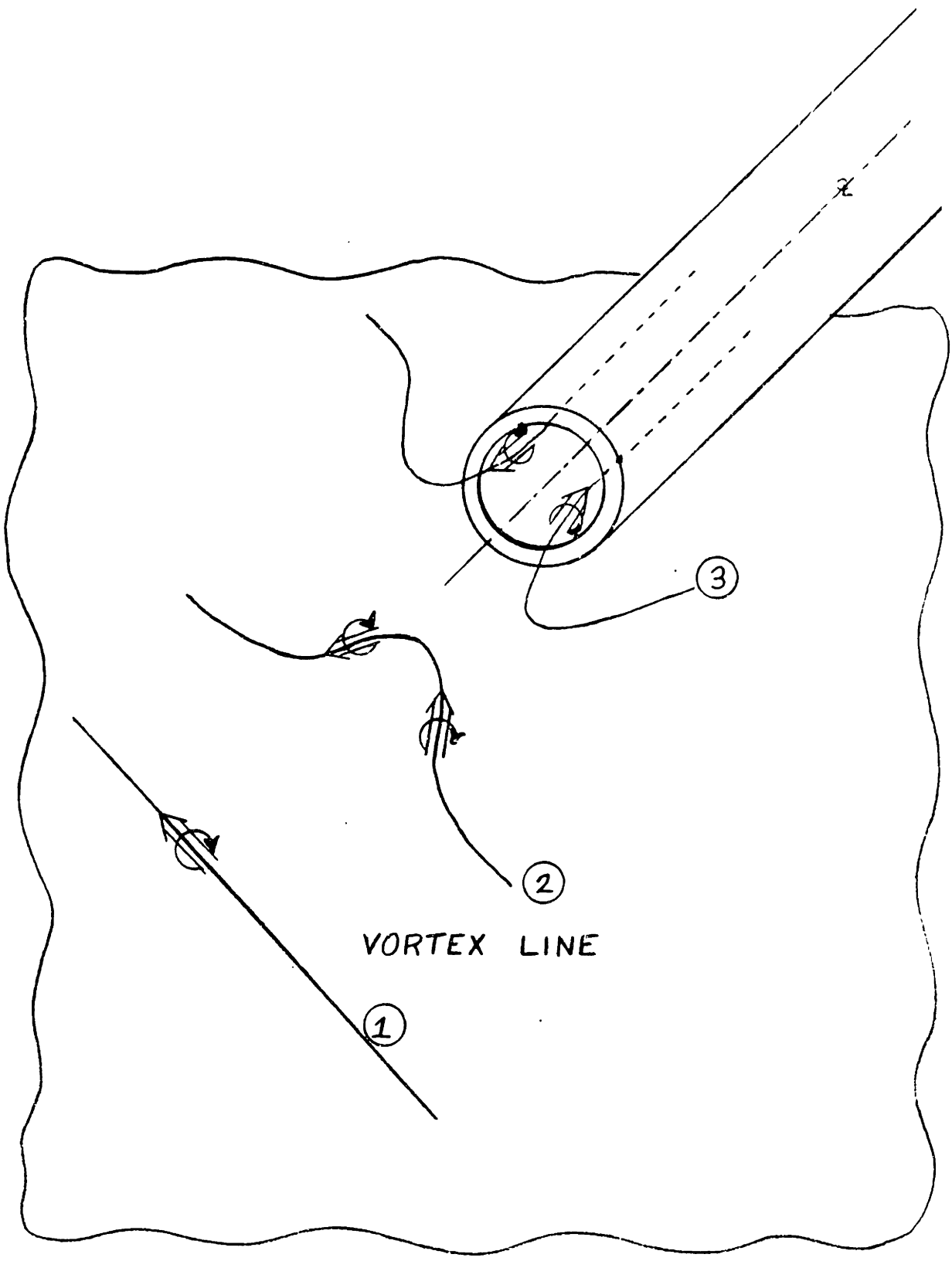

FIGURE 1: Suggested Sketch of a Vortex Line at Three Instants of Time

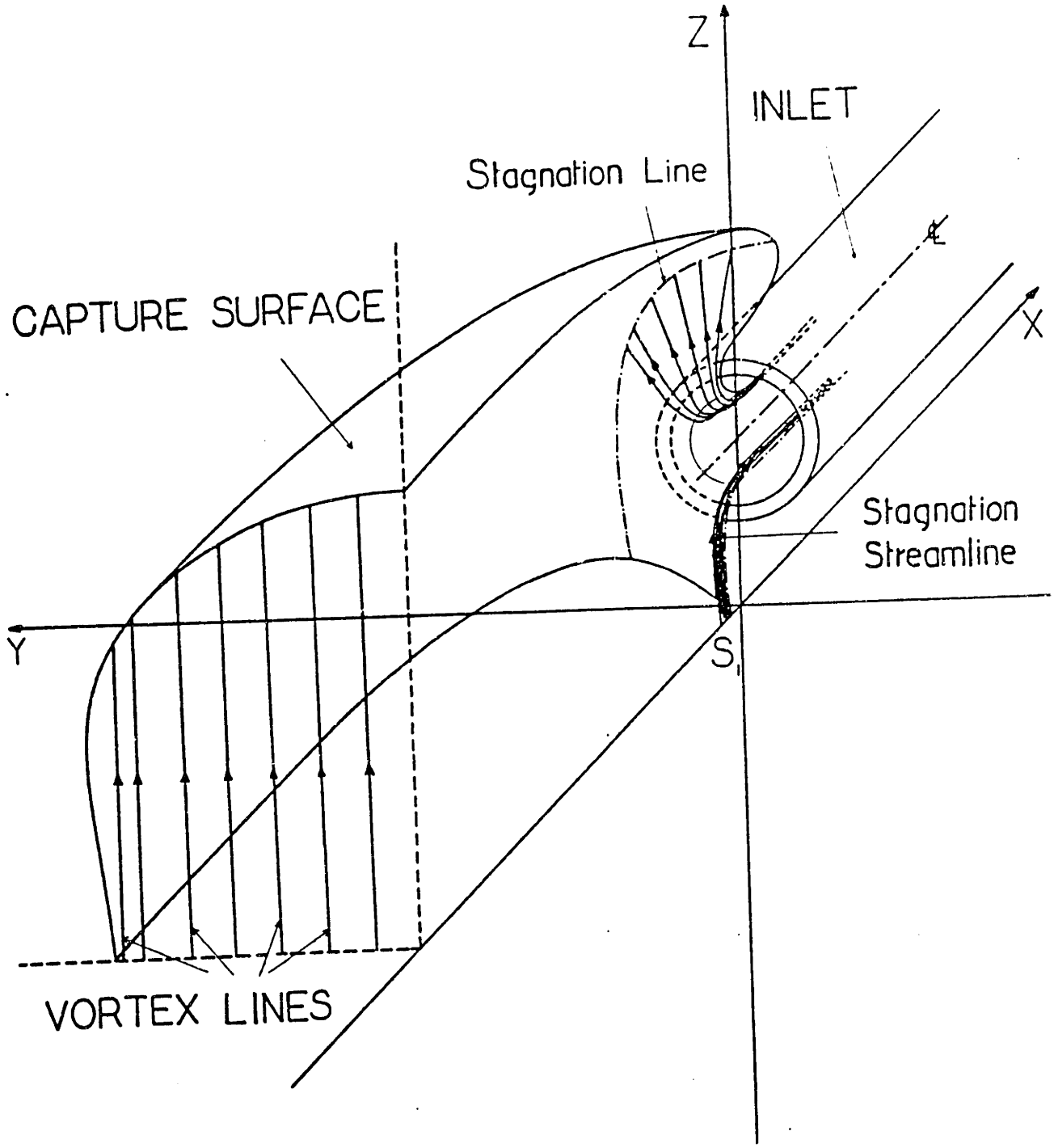

FIGURE 2: Suggested Deformation of a Far Upstream Uniform Distribution of Vertical Vortex Lines, Case 1: Viguier's Results (1)

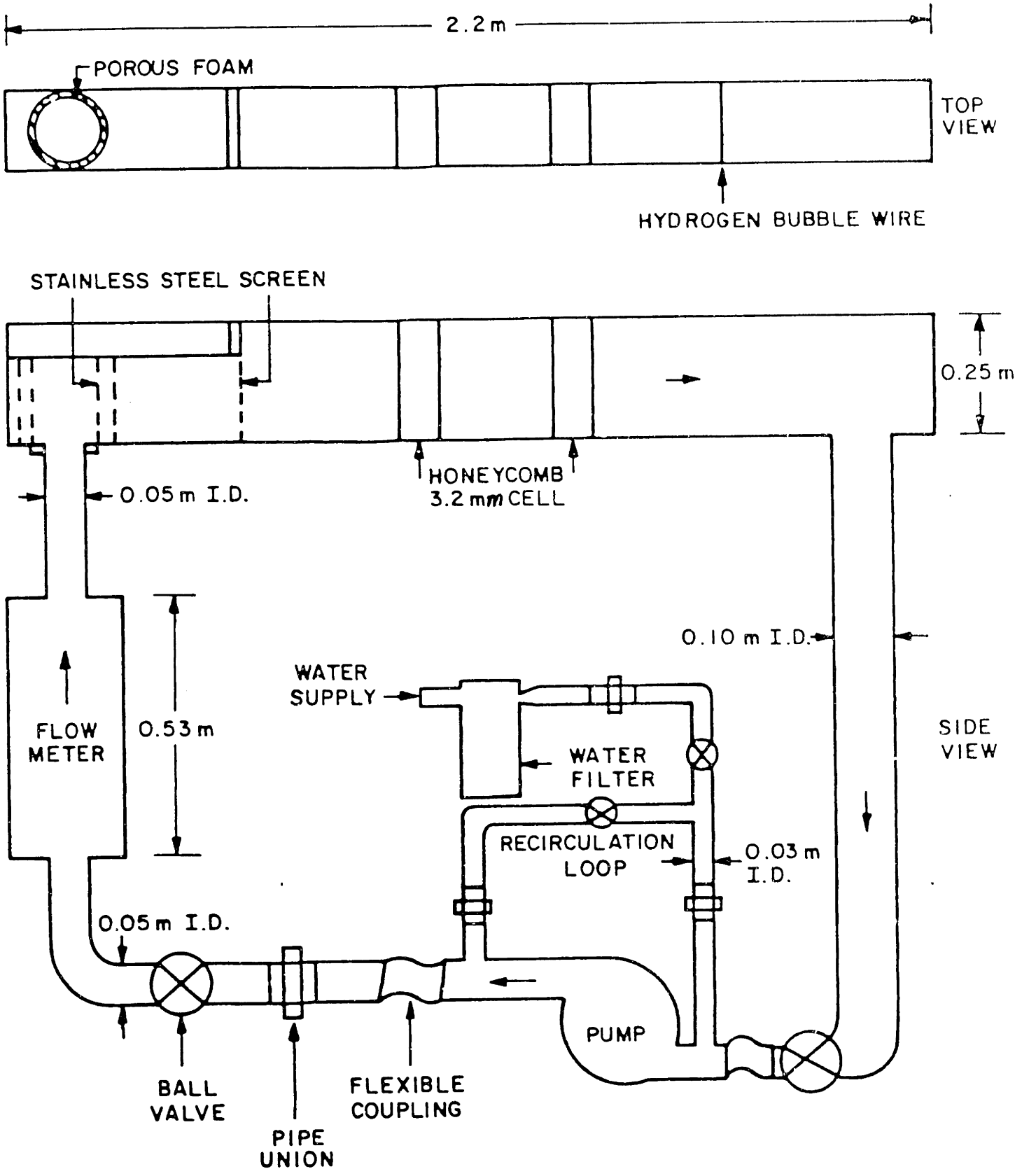

FIGURE 3: Sketch of the G.T. & P.D.L. Small Water Tunnel

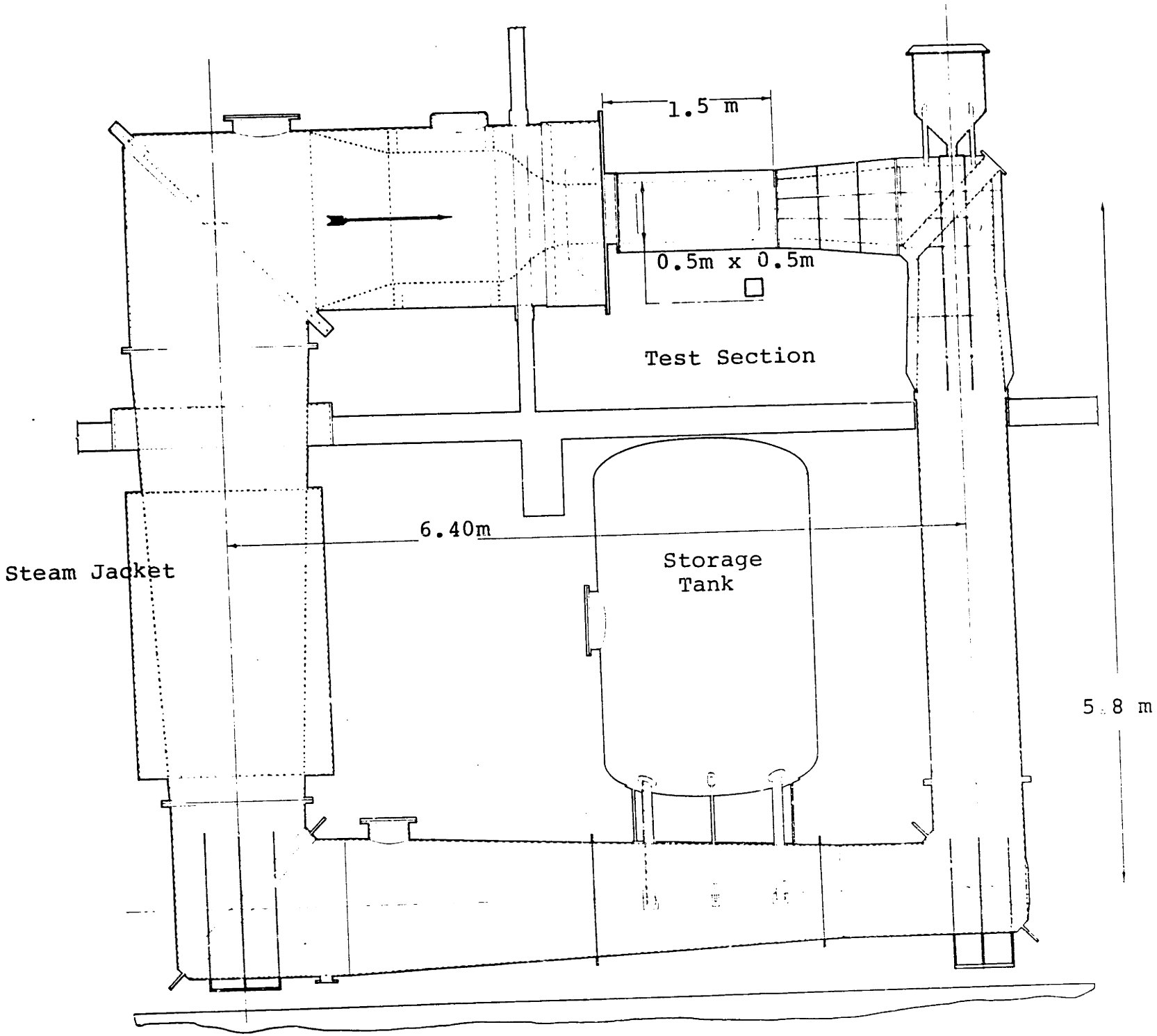
1.5 m
0.5m x 0.5m
Test Section
6.40m
Steam Jacket
Storage
Tank
5.8 m

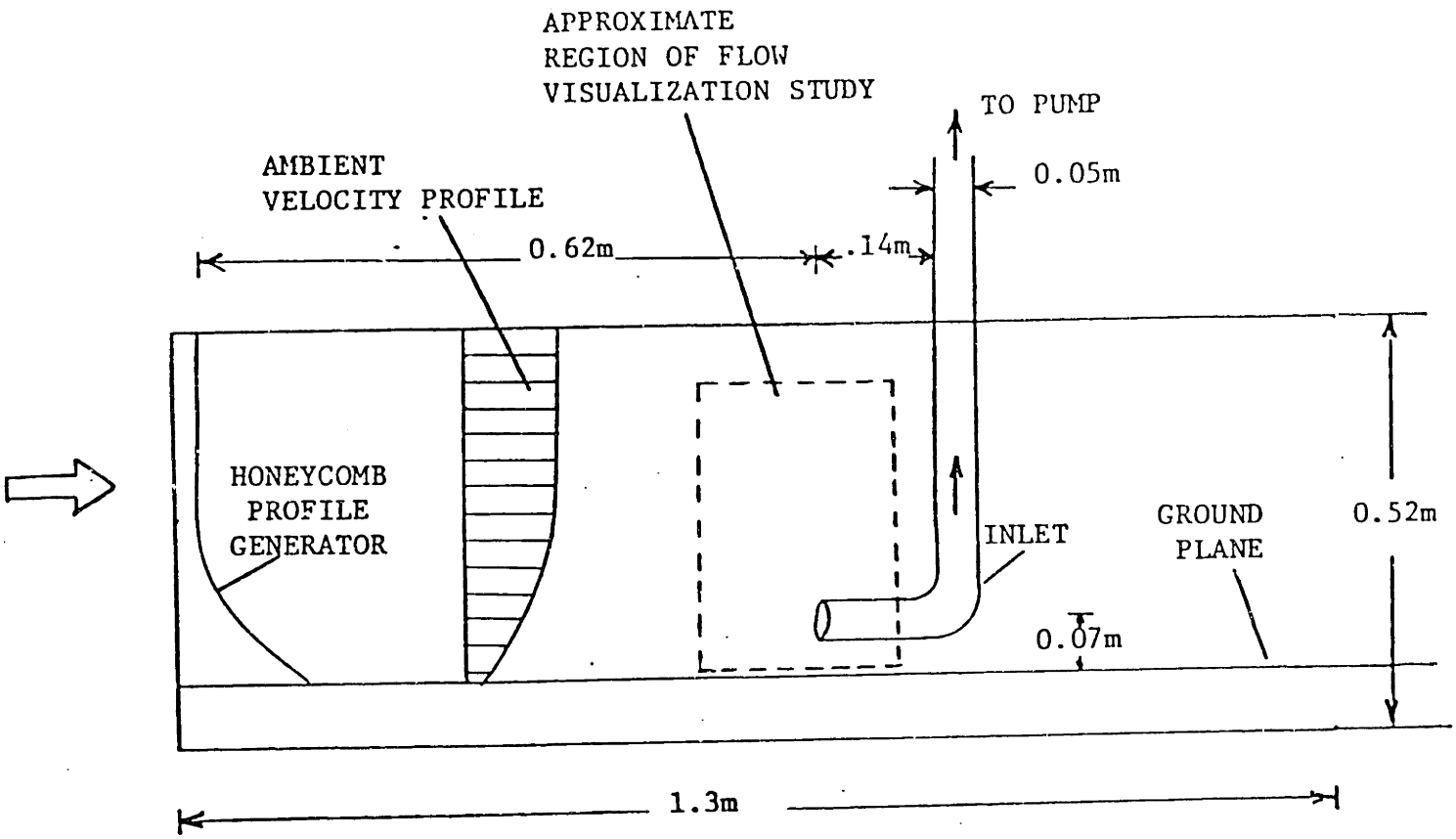

FIGURE 5: Sketch of Water Tunnel Test Section with Inlet Oriented at 0^{o} to the Mean Flow in a Boundary Layer Type Shear Flow

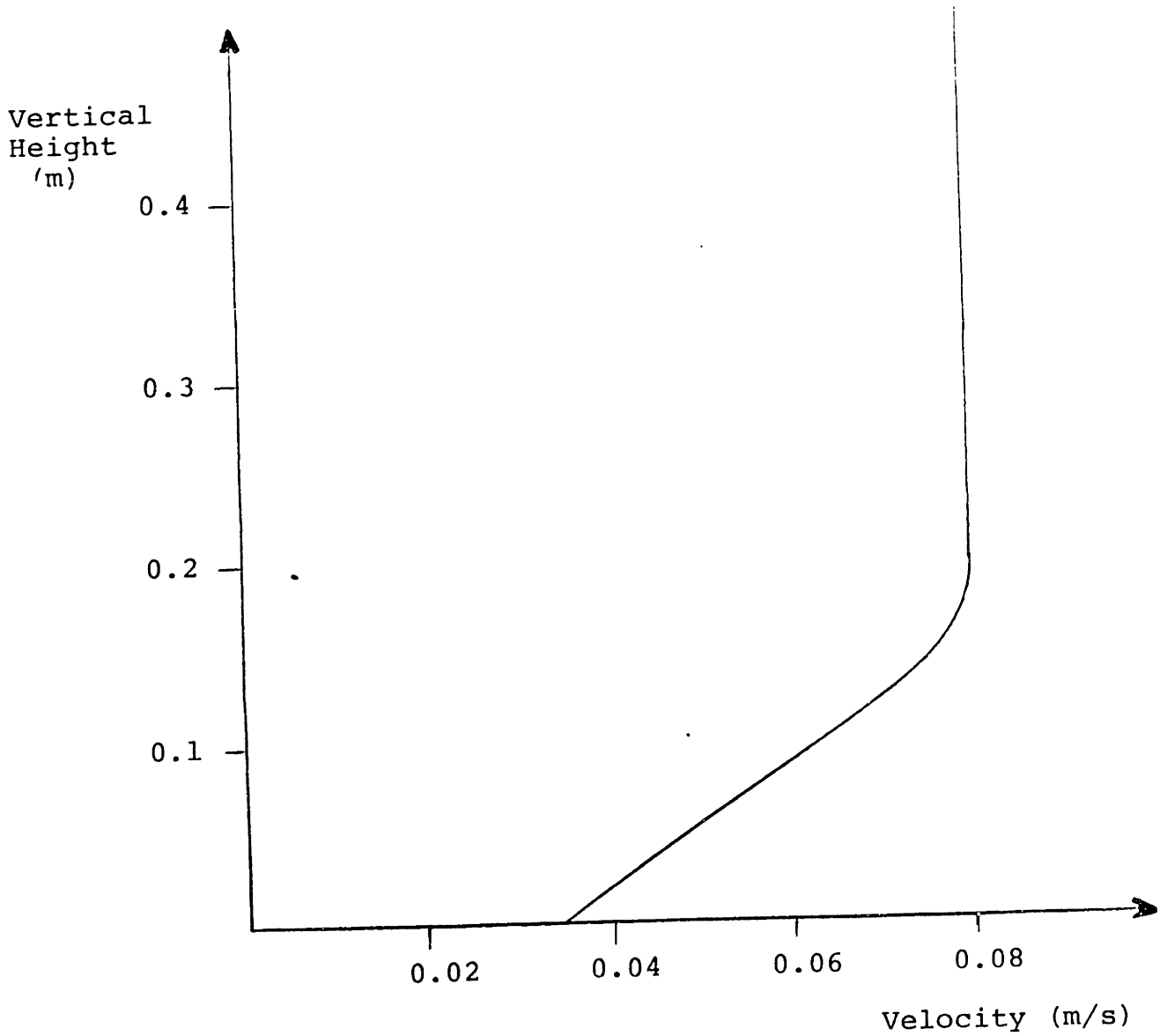

FIGURE 6: Boundary Layer Type Profile (Calculated from Hydrogen Bubble Flow Visualization)

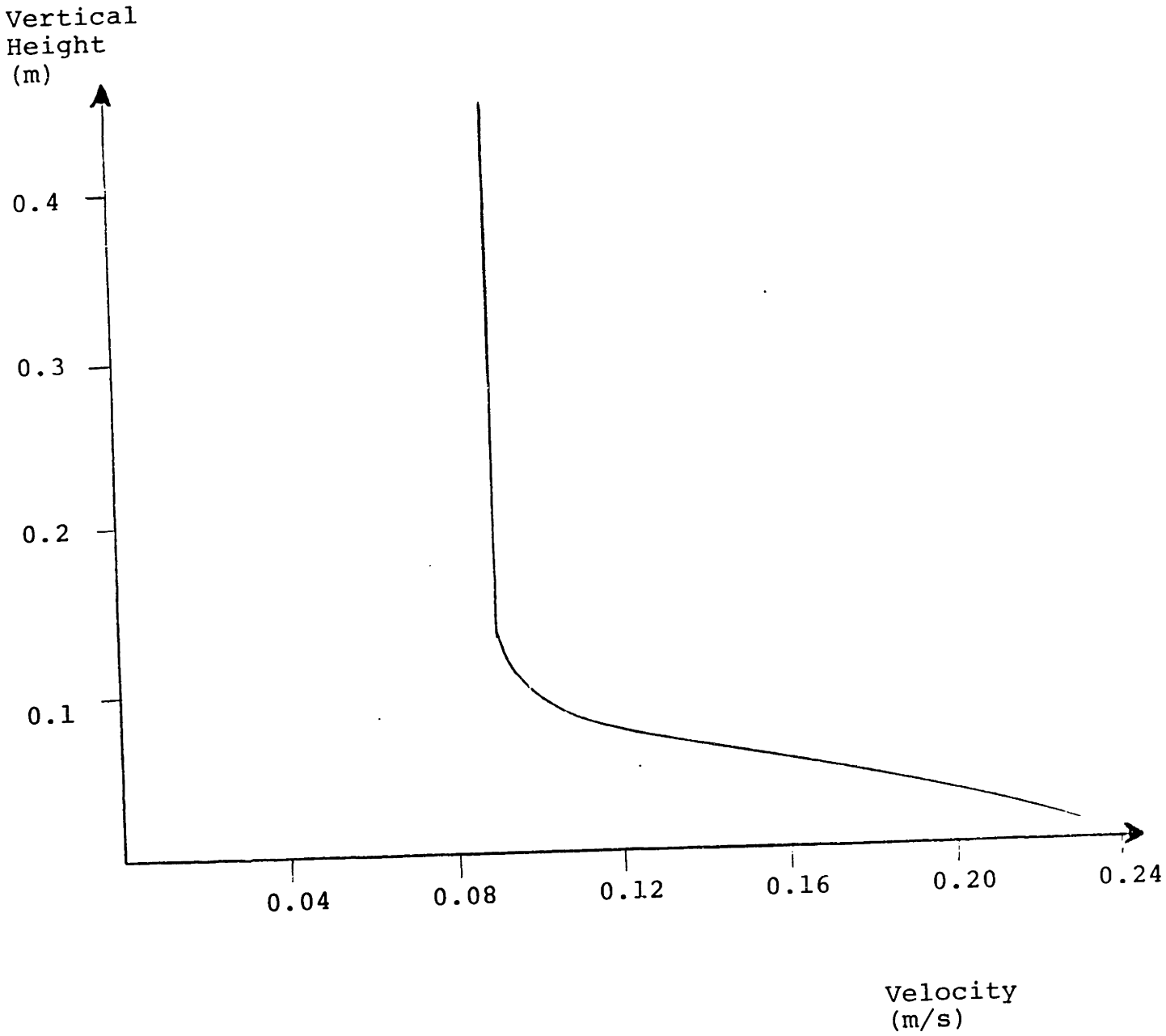

FIGURE 7: Jet Type Profile (Calculated from Hydrogen Bubble Flow Visualization)

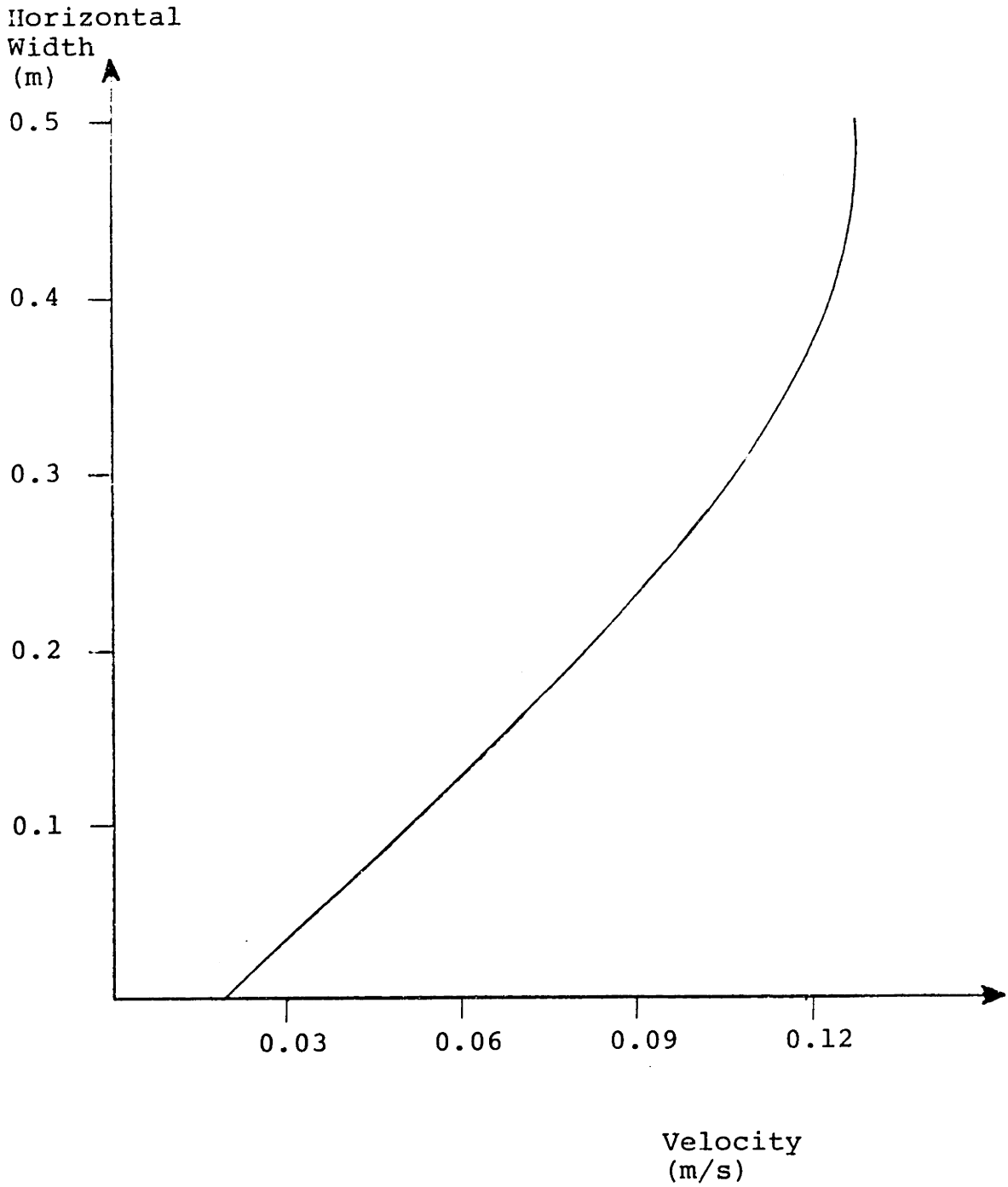

FIGURE 8: Right to Left Windshear Profile (Calculated from Hydrogen Bubble Flow Visualization)

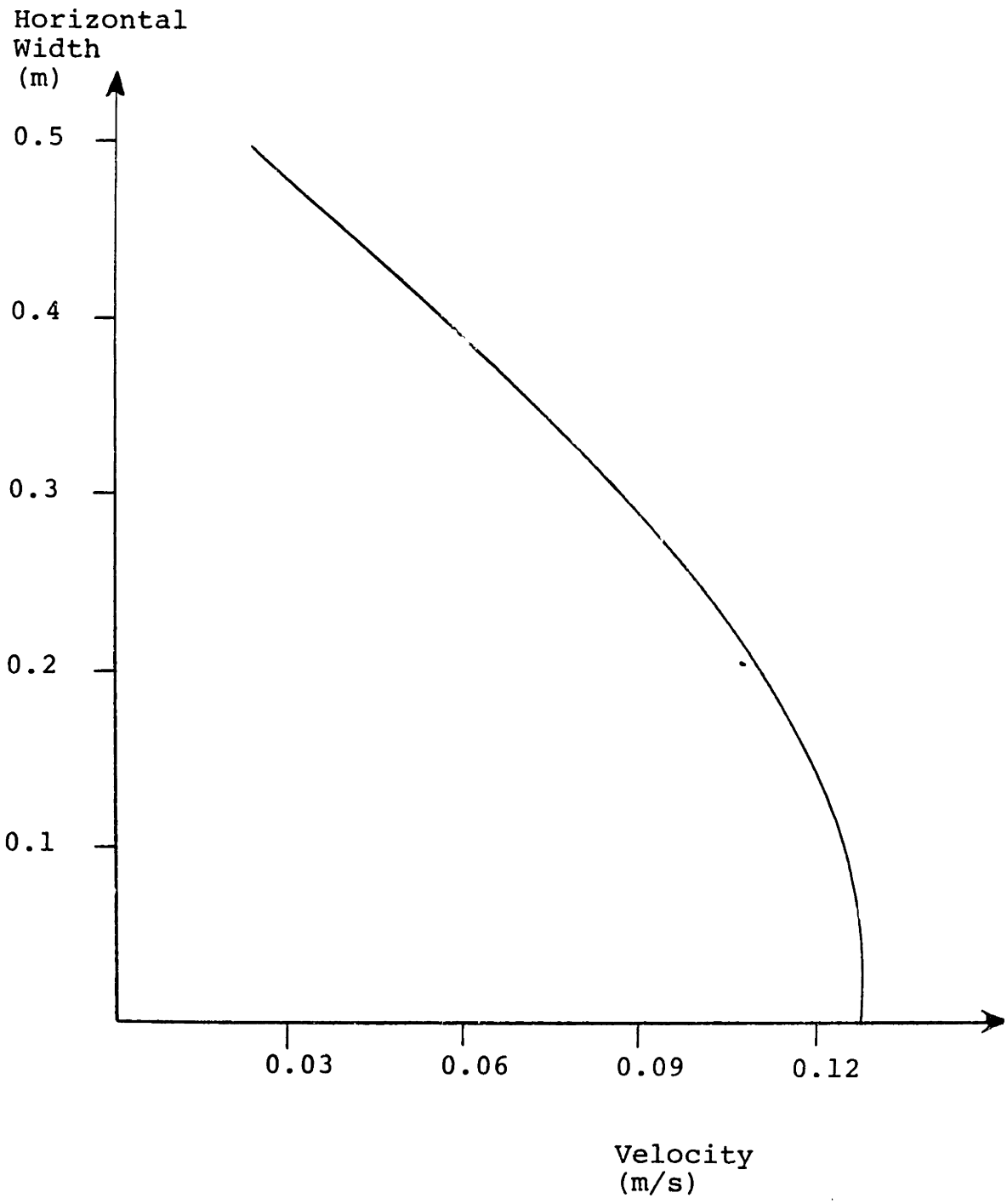

FIGURE 9: Left to Right Windshear Profile (Calculated from Hydrogen Bubble Flow Visualization)

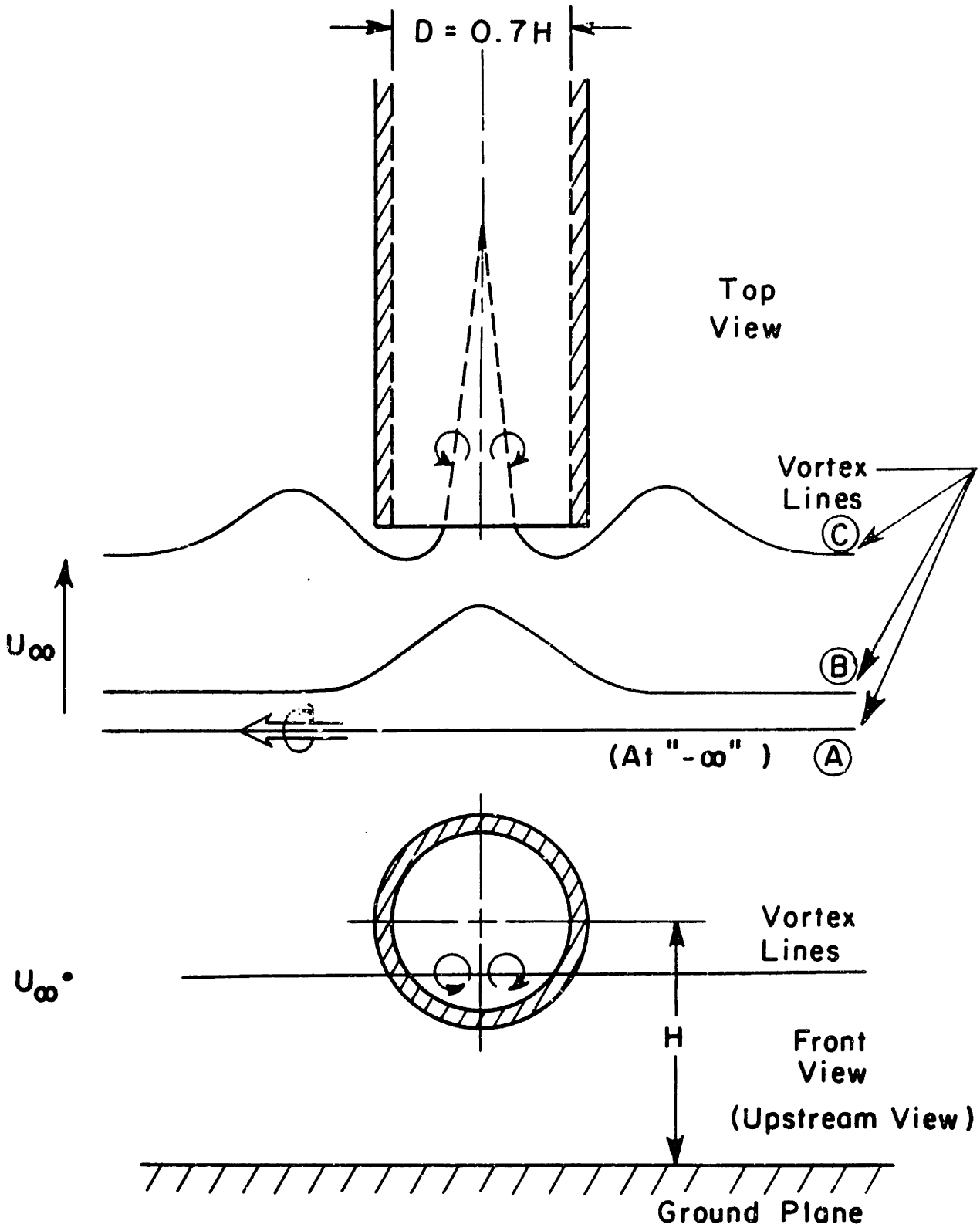

FIGURE 10: Ingestion of Horizontal Vortex Lines into a 0^o Inlet for Three Instants of Time
(Drawn from Hydrogen Bubble Flow Visualization)

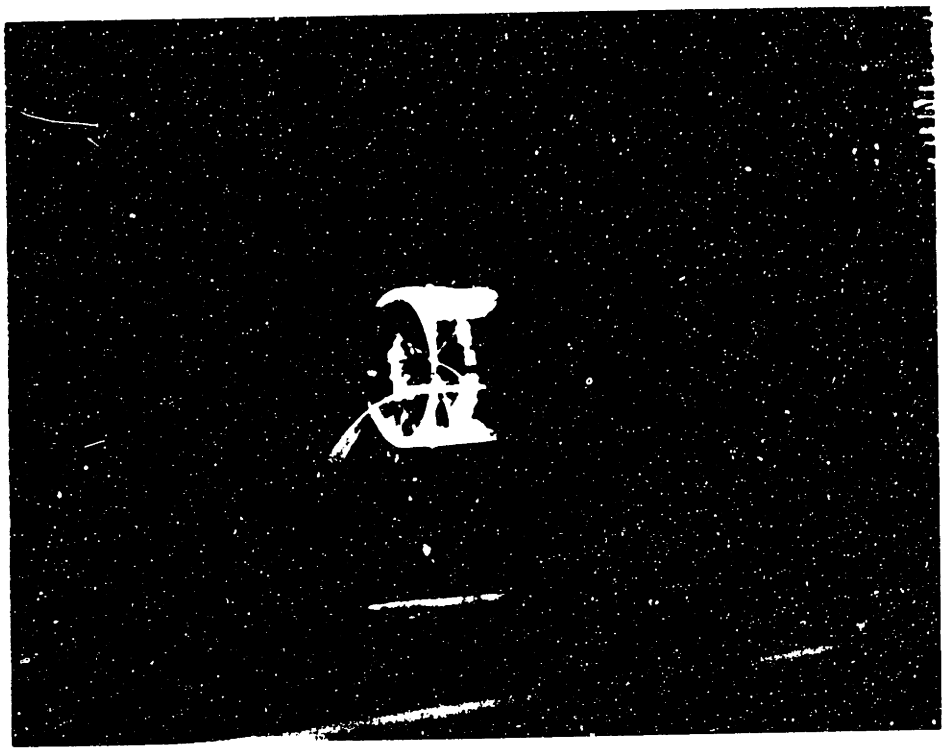

FIGURE 11a

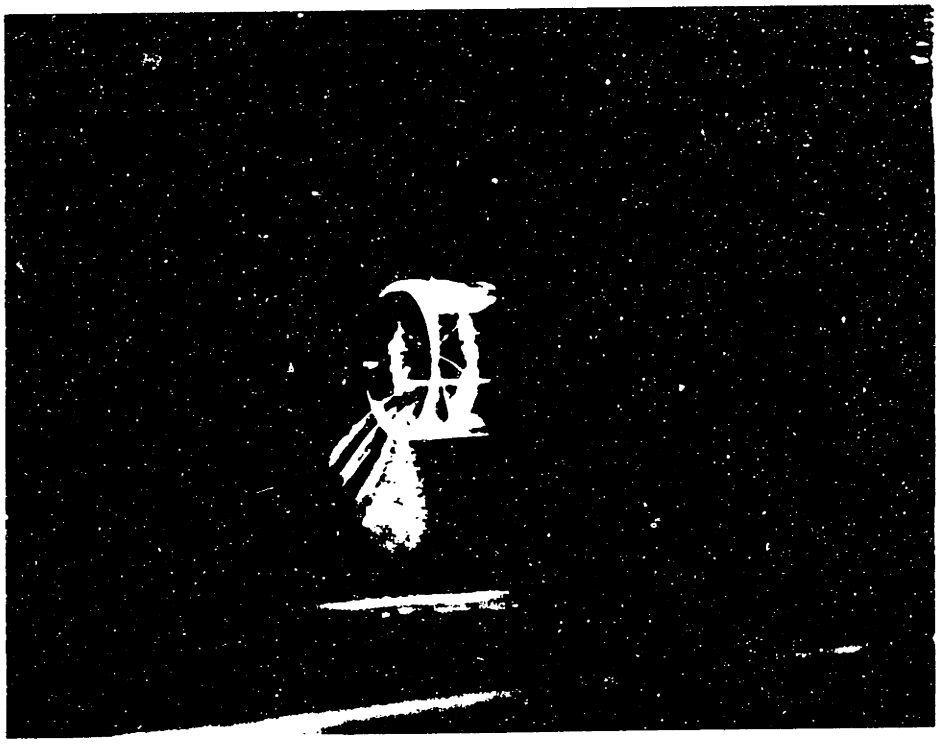

FIGURE 11b

FIGURE 11(a-c): Ingestion of Horizontal Vortex Lines Into a 0° Inlet for Three Successive Time Intervals, $t_a < t_b < t_c$

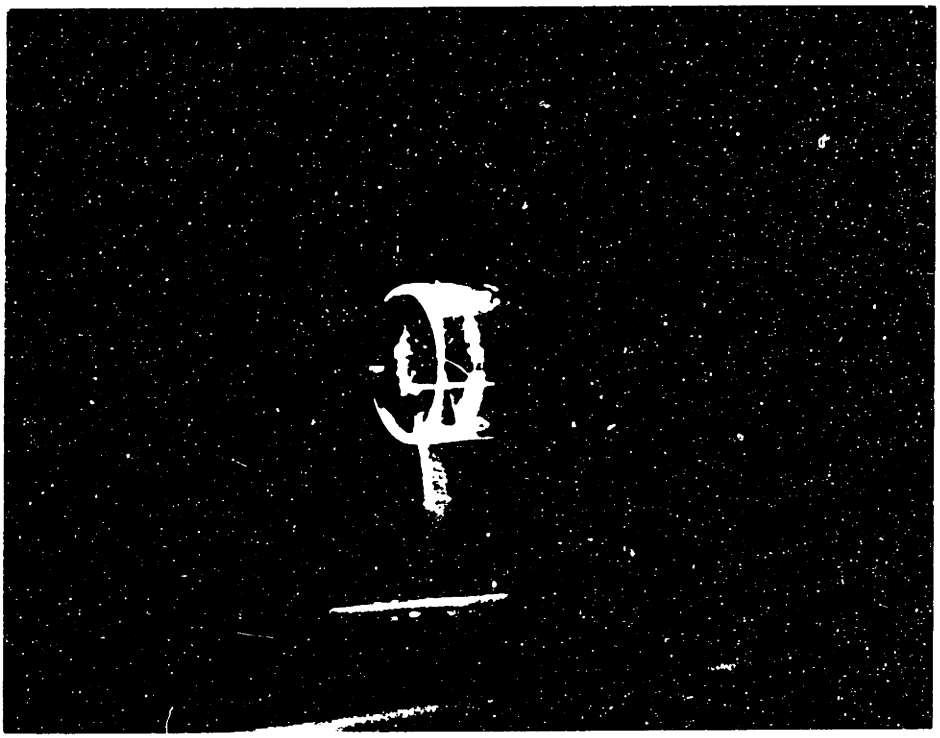

FIGURE 11c

FIGURE 11(a-c): Ingestion of Horizontal Vortex Lines Into a 0^{o} Inlet for Three Successive Time Intervals, $t_a < t_b < t_c$

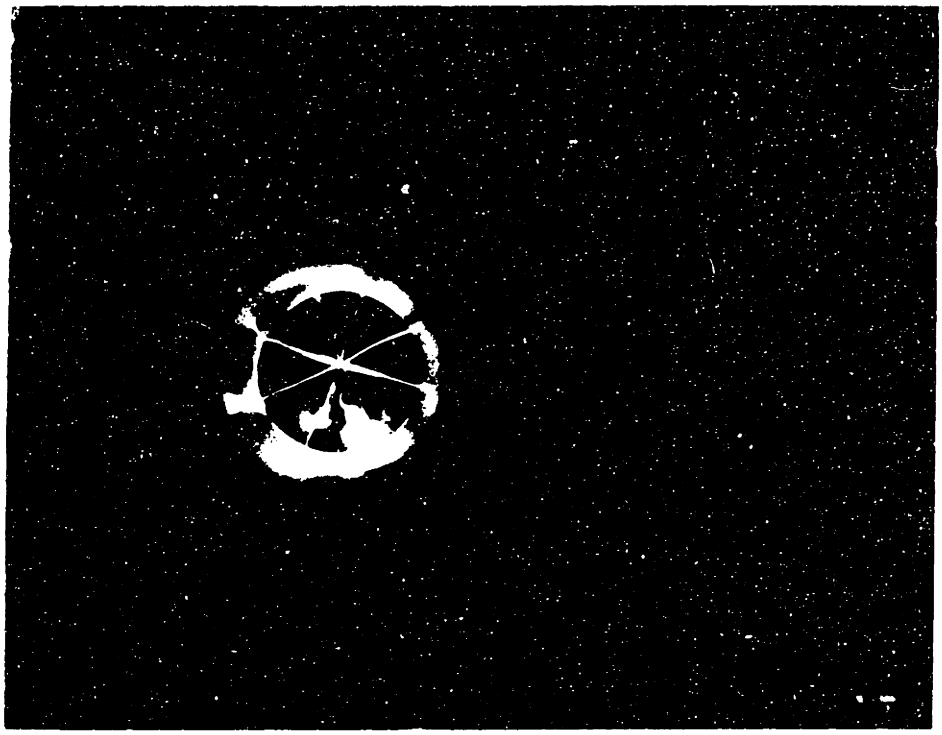

FIGURE 12

FIGURE 12: Ingestion of a Horizontal Vortex Line Into a 0^{o} Inlet - Viewed Looking into the Inlet
(Photograph of Hydrogen Bubble Flow Visualization)

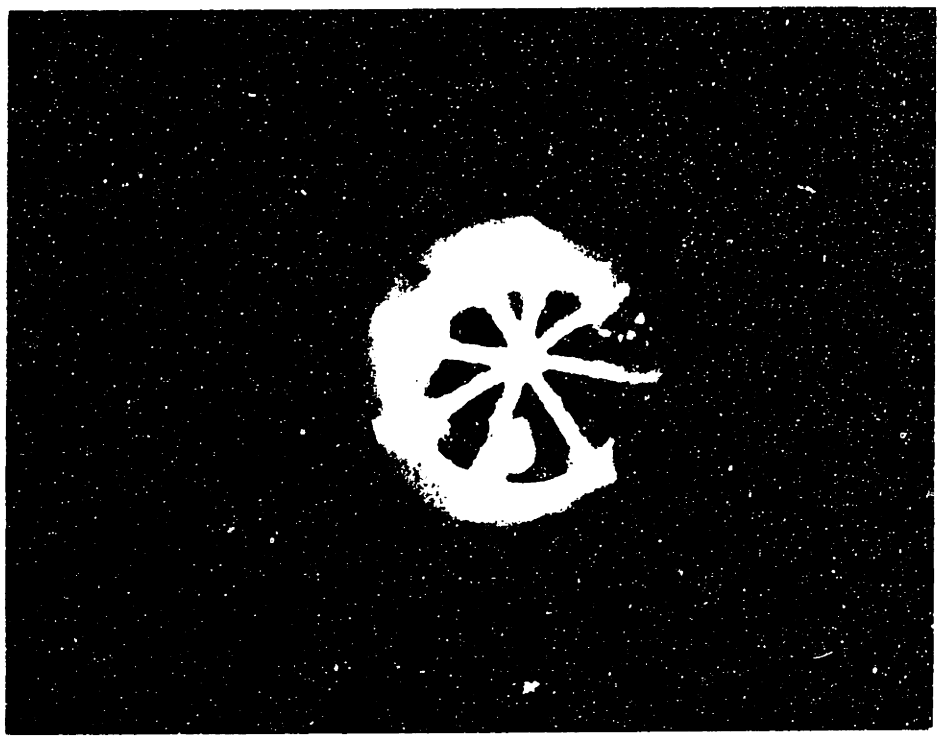

FIGURE 13

FIGURE 13: Ingestion of a Vertical Vortex Line, Associated with a Right to Left Shear, Into a 0^{o} Inlet - Viewed Looking into the Inlet
(Photograph of Hydrogen Bubble Flow Visualization)

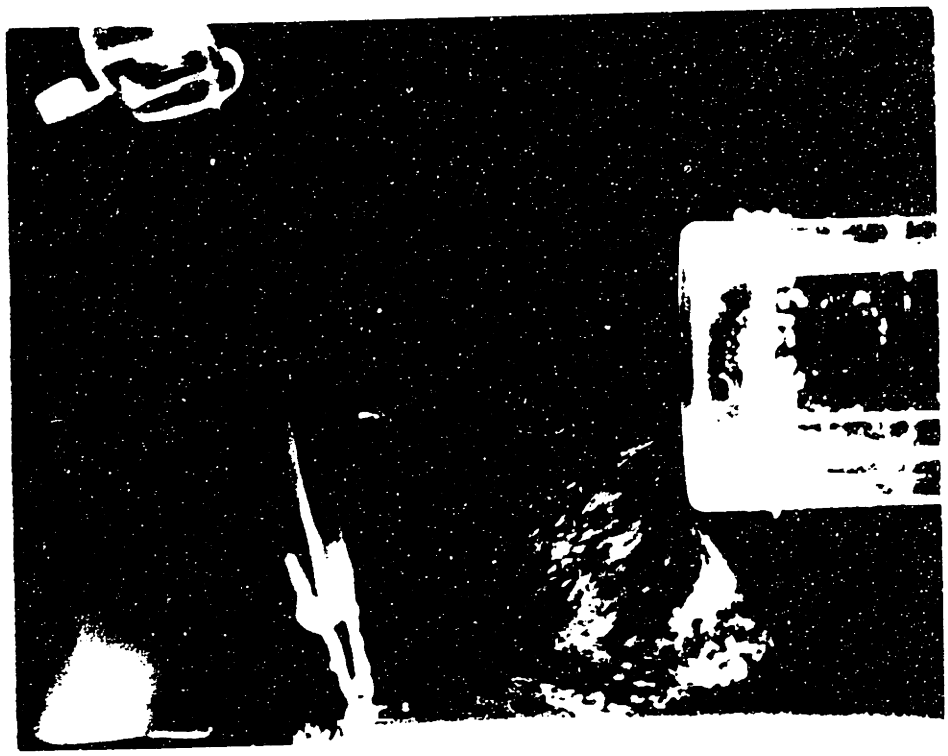

FIGURE 14

FIGURE 14: Vertical Vortex Leg Extending Between the Ground Plane and 0^{o} Inlet (Photograph of Hydrogen Bubble Flow Visualization)

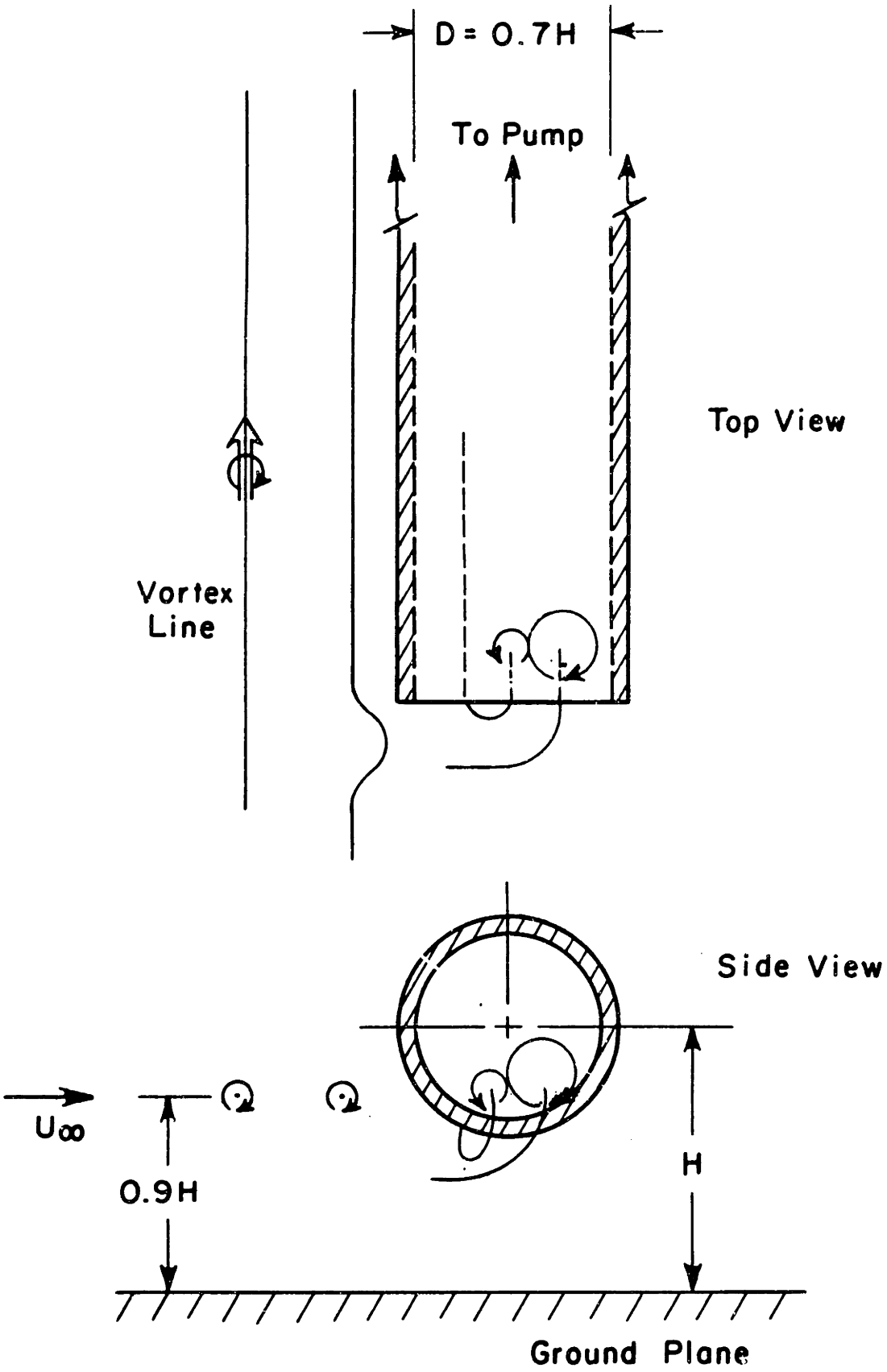

FIGURE 15: Ingestion of Horizontal Vortex Lines Originating at 0.9H into a 90° Inlet (Drawn from Hydrogen Bubble Flow Visualization)

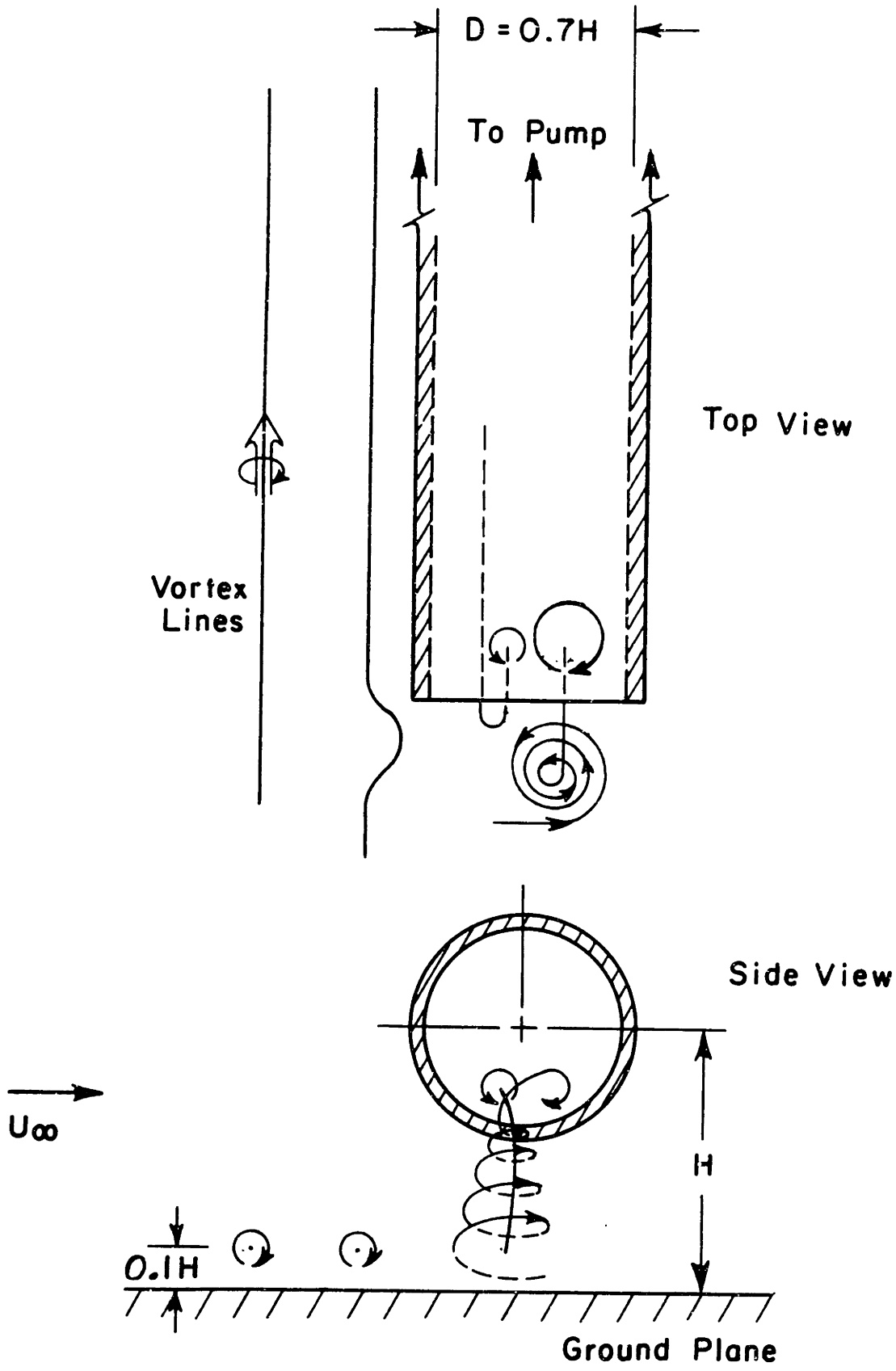

FIGURE 16: Ingestion of Horizontal Vortex Lines Originating at 0.1H into a 90° Inlet (Drawn from Hydrogen Bubble Flow Visualization)

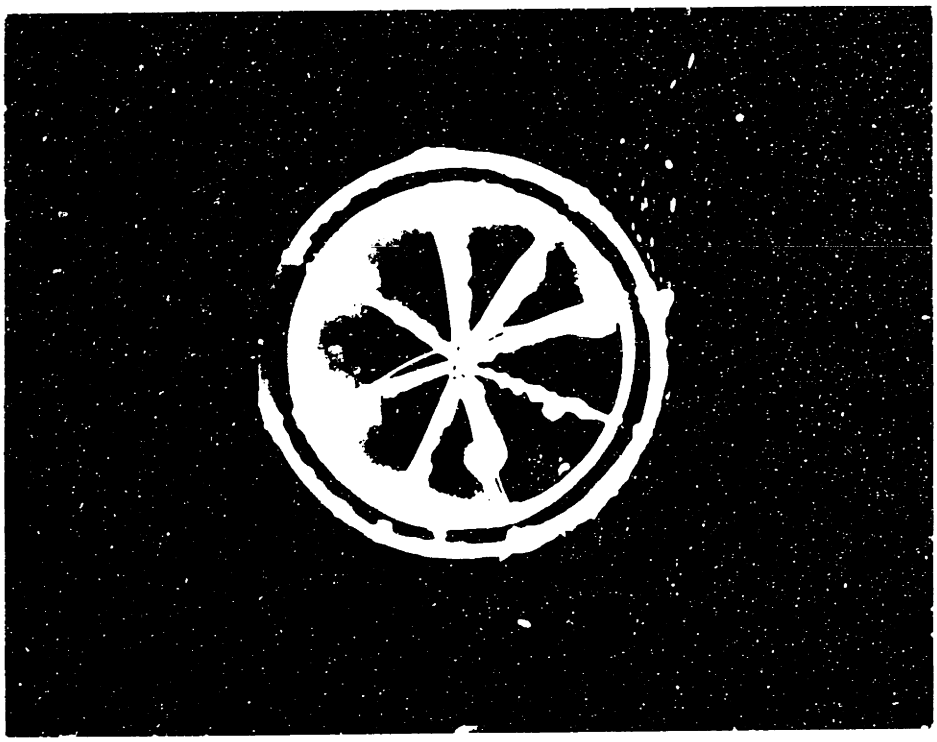

FIGURE 17

FIGURE 17: Ingestion of Vertical Vortex Lines Associated with the Left to Right Shear into a 90^{o} Inlet (Photograph of Hydrogen Bubble Flow Visualization)

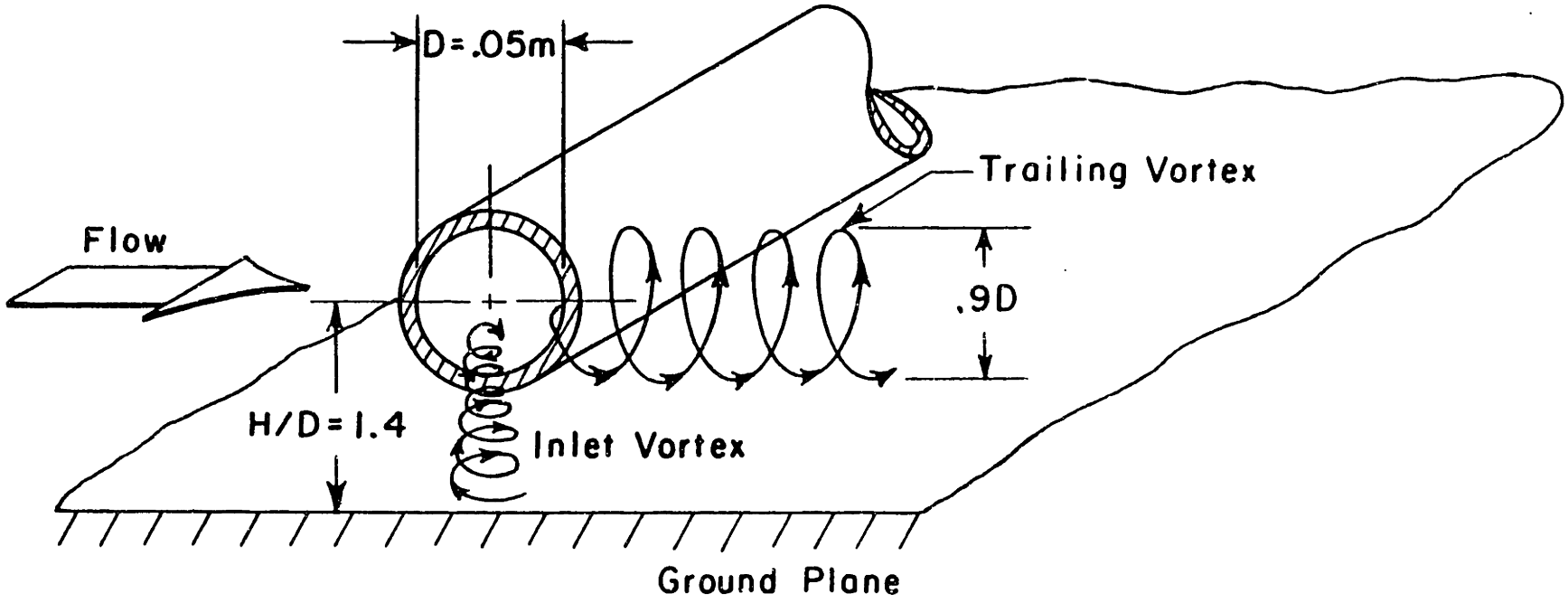

FIGURE 18: Streamlines Associated with a 90° Inlet in Irrotational Upstream Flow (Drawn from Hydrogen Bubble Flow Visualization)

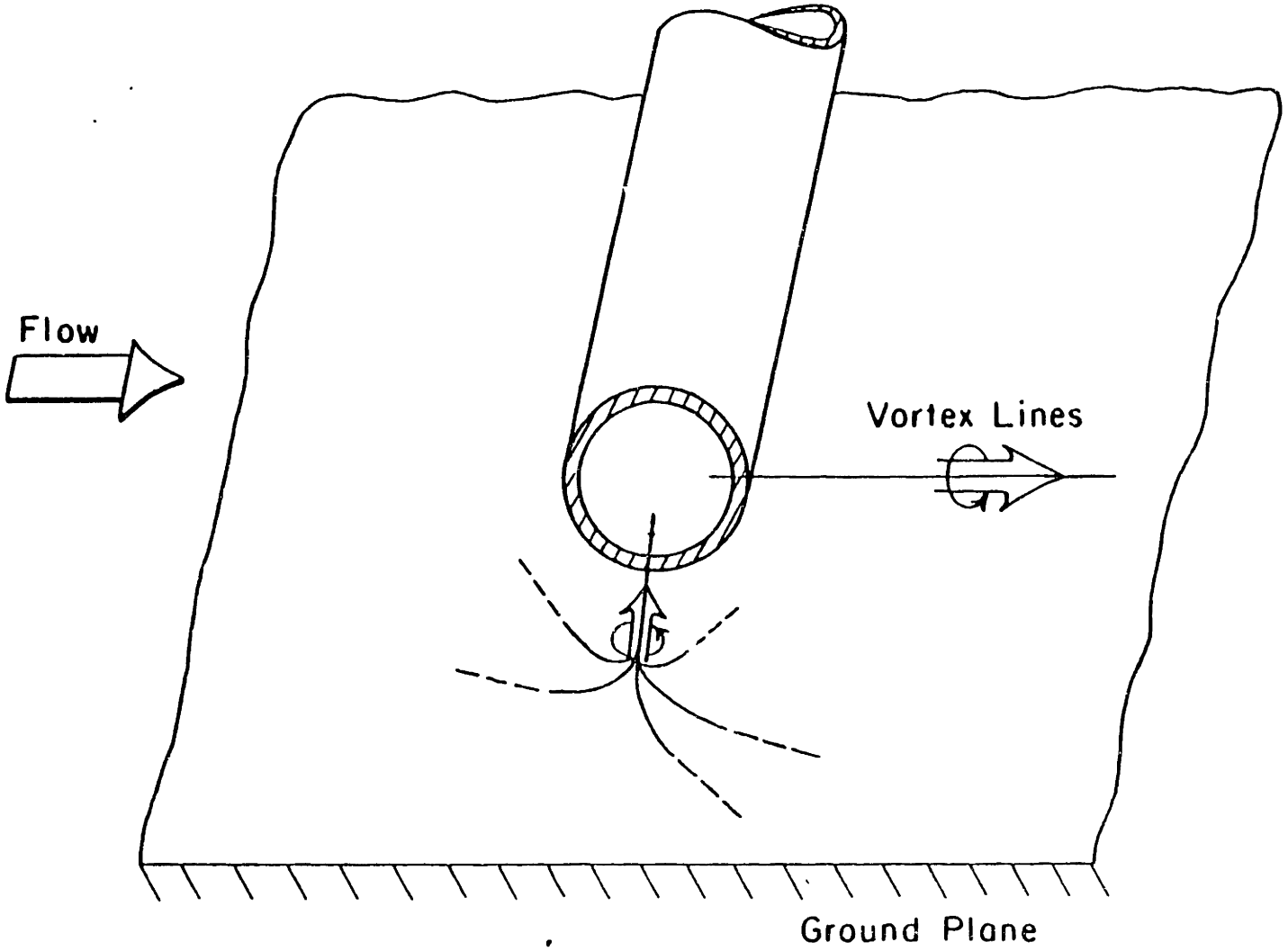

FIGURE 19: Vortex Lines Associated with a 90° Inlet in Irrotational Upstream Flow (Drawn from Hydrogen Bubble Flow Visualization)

(Drawn from Hydrogen Bubble Flow Visualization)

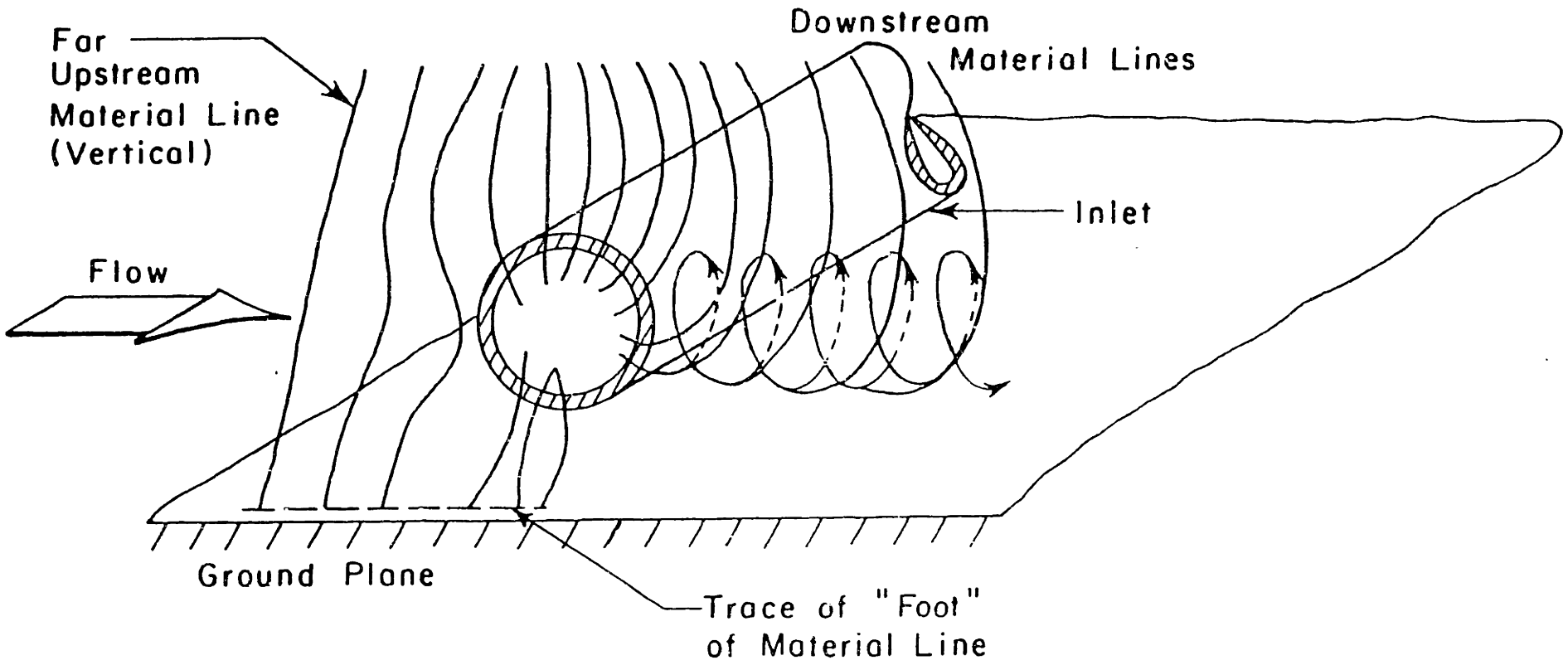

FIGURE 20: Material Lines Associated with a 90° Inlet in Irrotational Upstream Flow

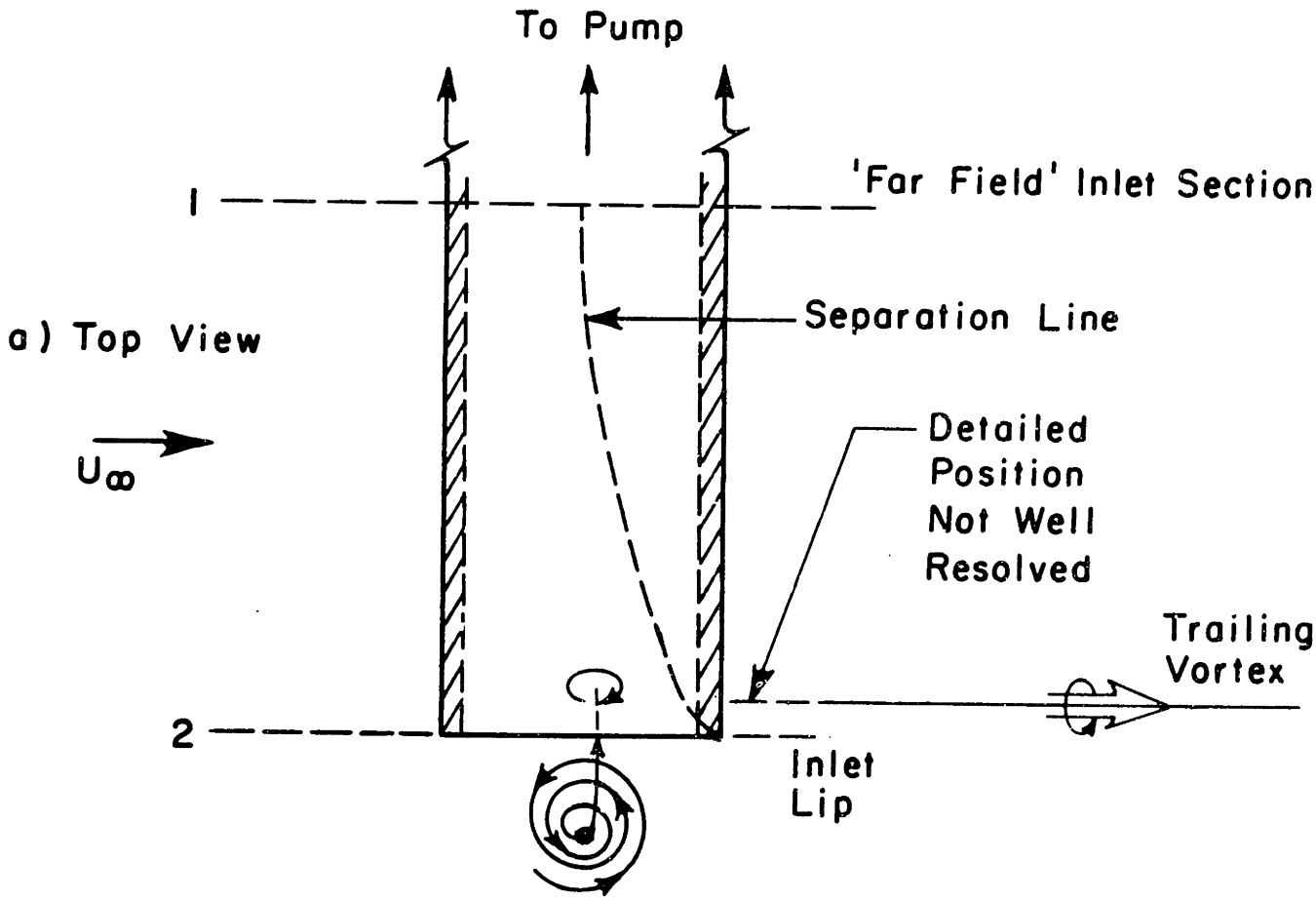

FIGURE 21(a-b): Variation of the Separation Point Along the Axial Length of a 90° Inlet in Irrotational Upstream Flow (Drawn from Hydrogen Bubble Flow Visualization)

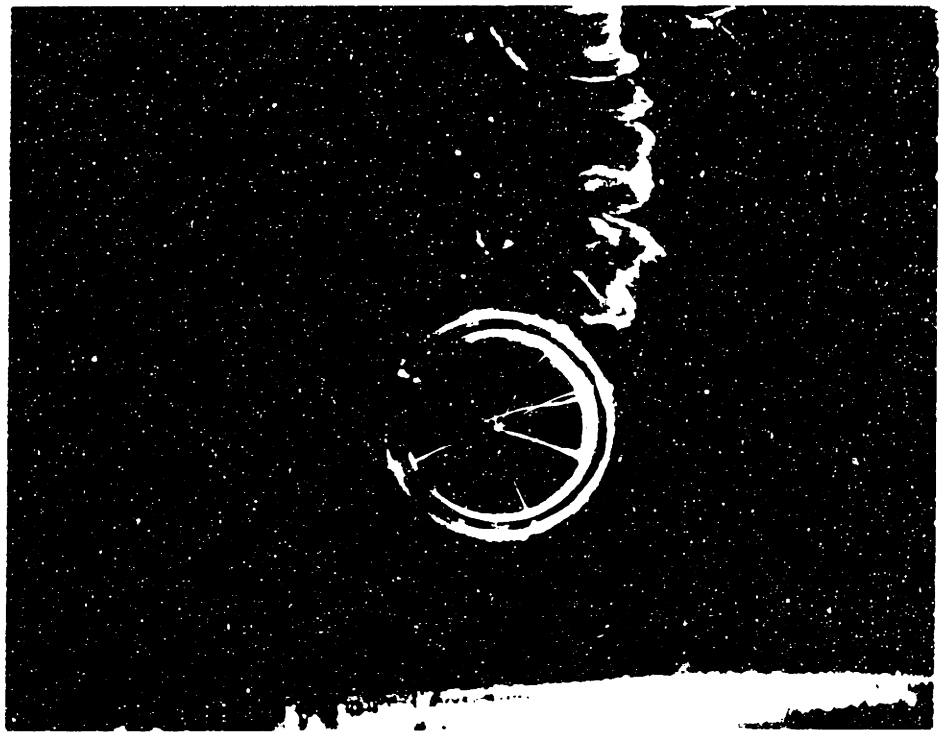

FIGURE 22a: High Value of U_i/U_∞, Symmetric Separation

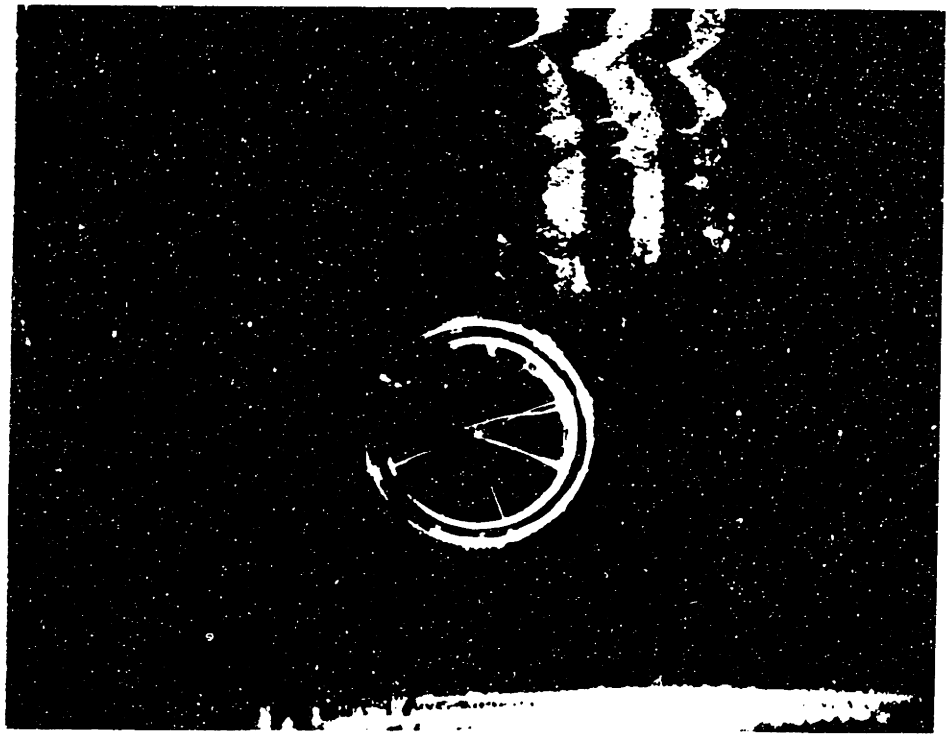

FIGURE 22b: First Intermediate Value of U_i/U_∞, Asymmetric Separation is Beginning

FIGURE 22(a-d): Successive Shifting of the Inlet Lip's Separation Point for 90^o Inlet in Transient Irrotational Upstream Flow (Photograph of Hydrogen Bubble Flow Visualization)

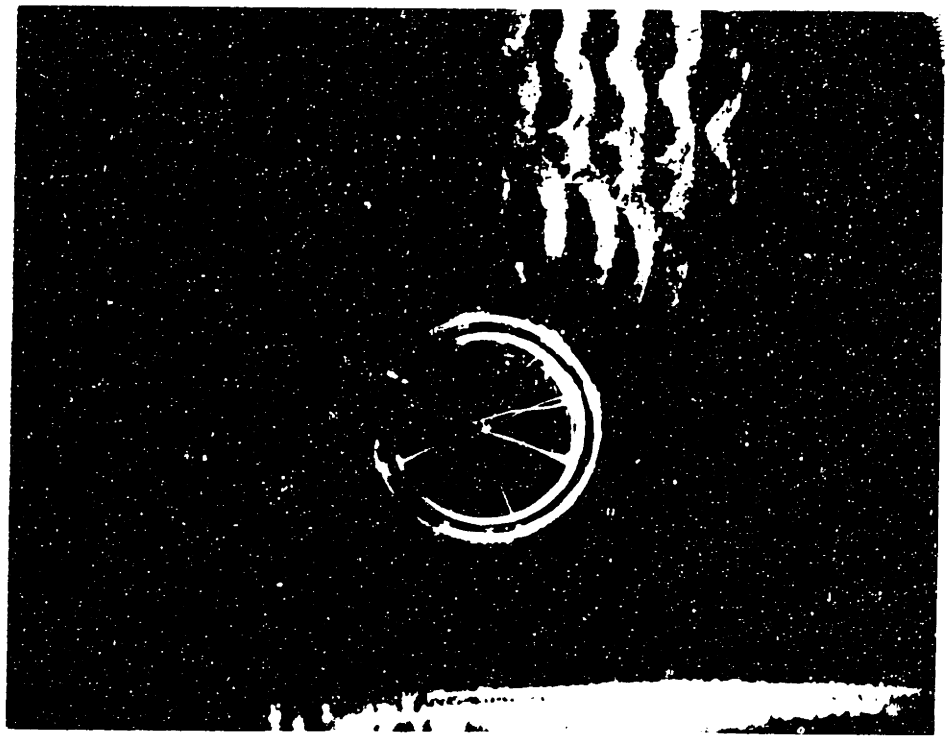

FIGURE 22c: Second Intermediate Value of U_i/U_∞, Asymmetric Separation

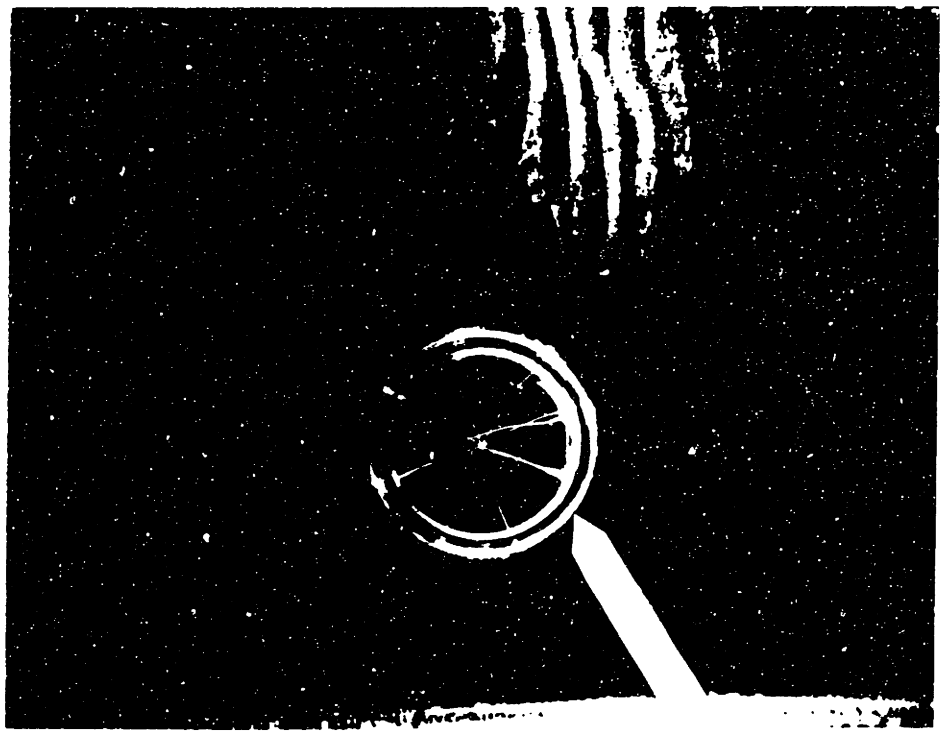

Separation Point

FIGURE 22d: Low Value of U_i/U_∞, Inlet Separation at 4:00

FIGURE 22(a-d): Successive Shifting of the Inlet Lip's Separation Point for 90^o Inlet in Transient Irrotational Upstream Flow (Photograph of Hydrogen Bubble Flow Visualization)

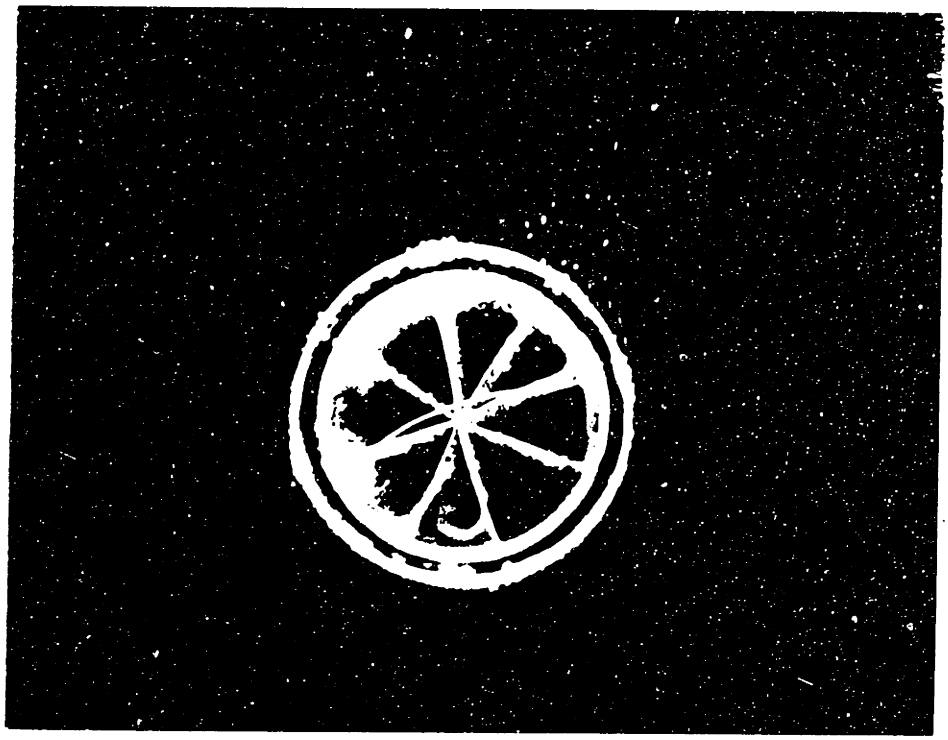

FIGURE 23: 90° Inlet in Transient Irrotational Upstream Flow (Photograph of Hydrogen Bubble Flow Visualization)

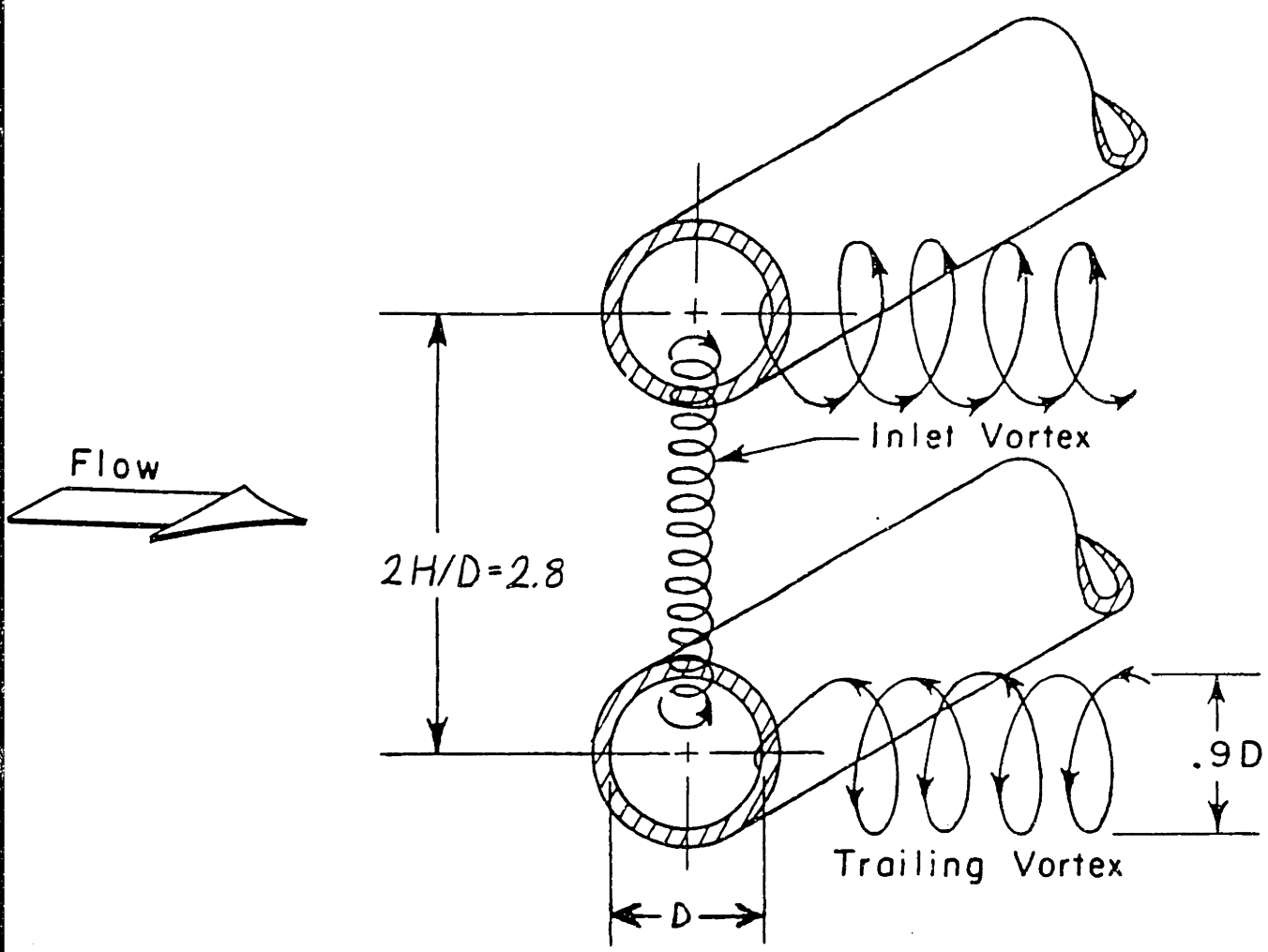

FIGURE 24: Streamlines Associated with 90° Double Inlet Configuration in Irrotational Upstream Flow (Drawn from Hydrogen Bubble Flow Visualization)

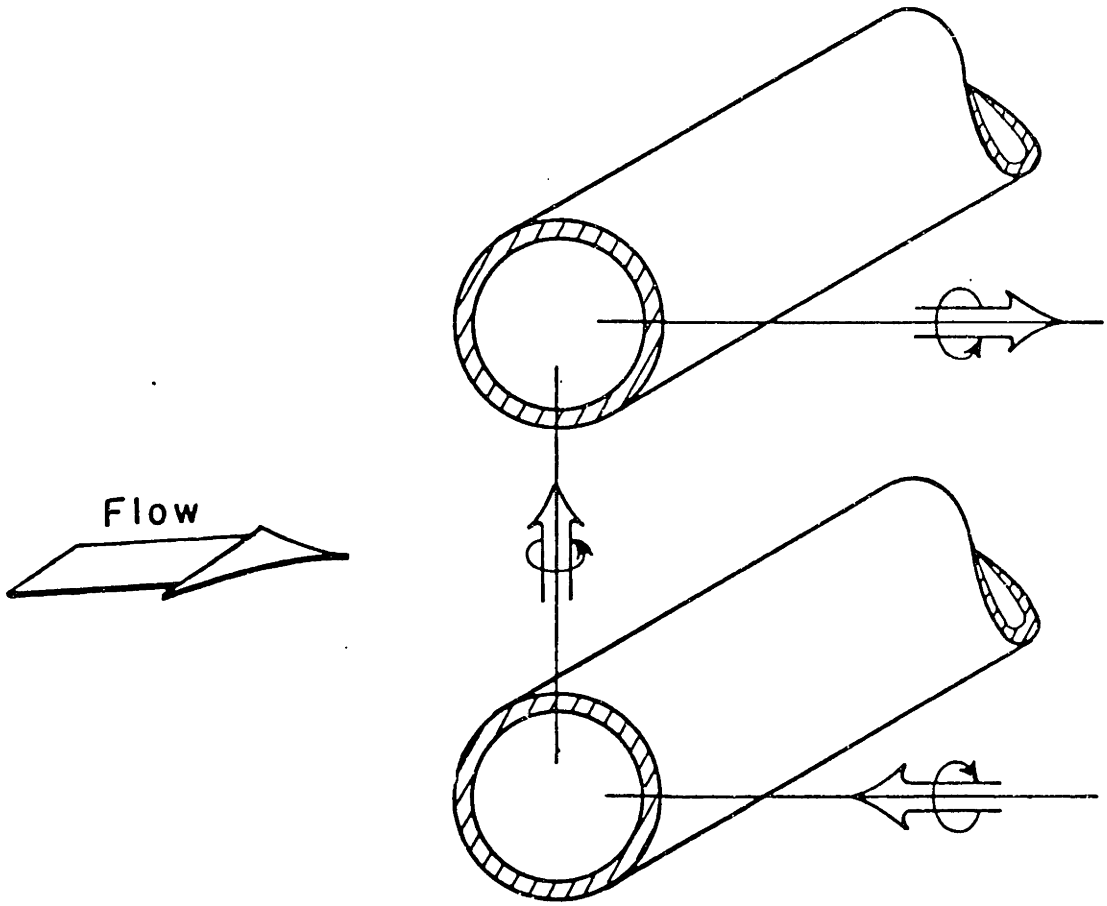

FIGURE 25: Vortex Lines Associated with 90° Double Inlet Configuration in Irrotational Upstream Flow (Drawn from Hydrogen Bubble Flow Visualization)

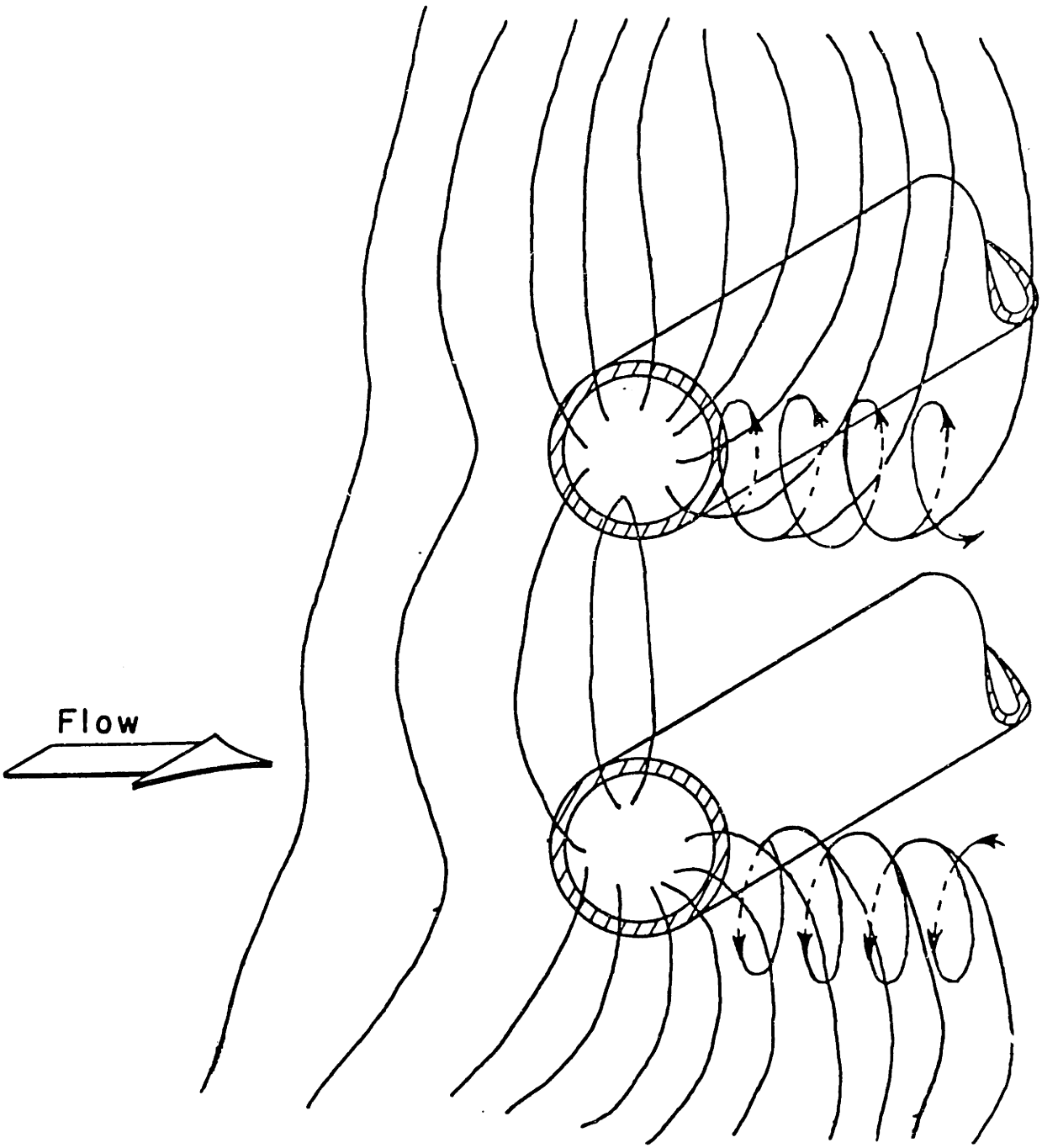

FIGURE 26: Material Lines Associated with 90° Double Inlet Configuration in Irrotational Upstream Flow (Drawn from Hydrogen Bubble Flow Visualization)

FIGURE 27: Material Lines Associated with 90° Double Inlet Configuration in Irrotational Upstream Flow (Photograph of Hydrogen Bubble Flow Visualization)

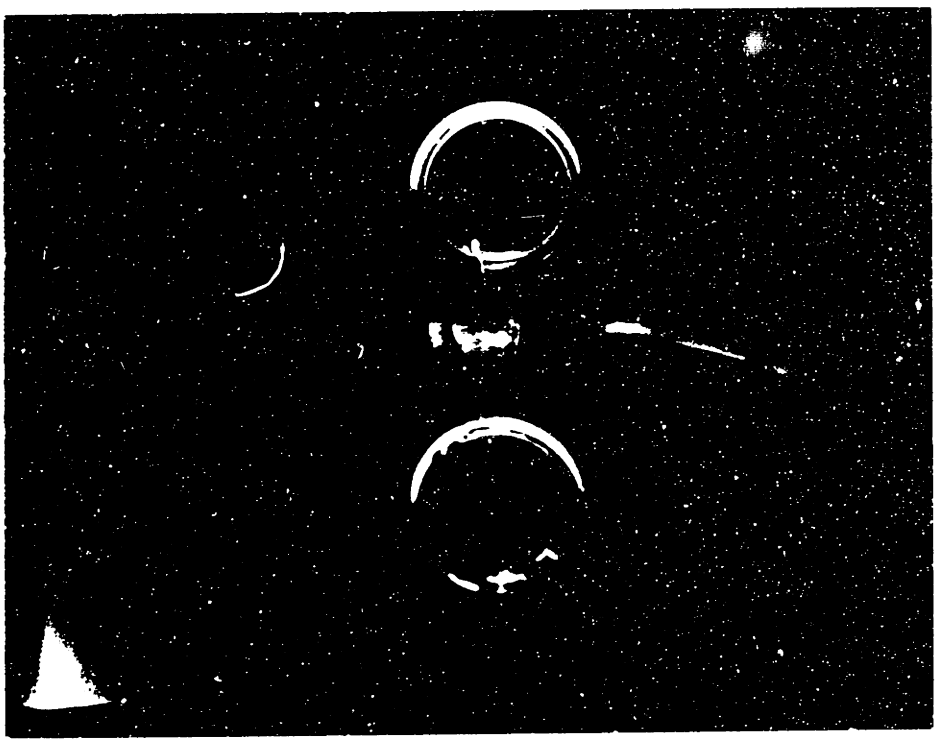

FIGURE 28: Vortex Core Extending Between Two 90° Inlets in Irrotational Upstream Flow (Photograph of Hydrogen Bubble Flow Visualization)

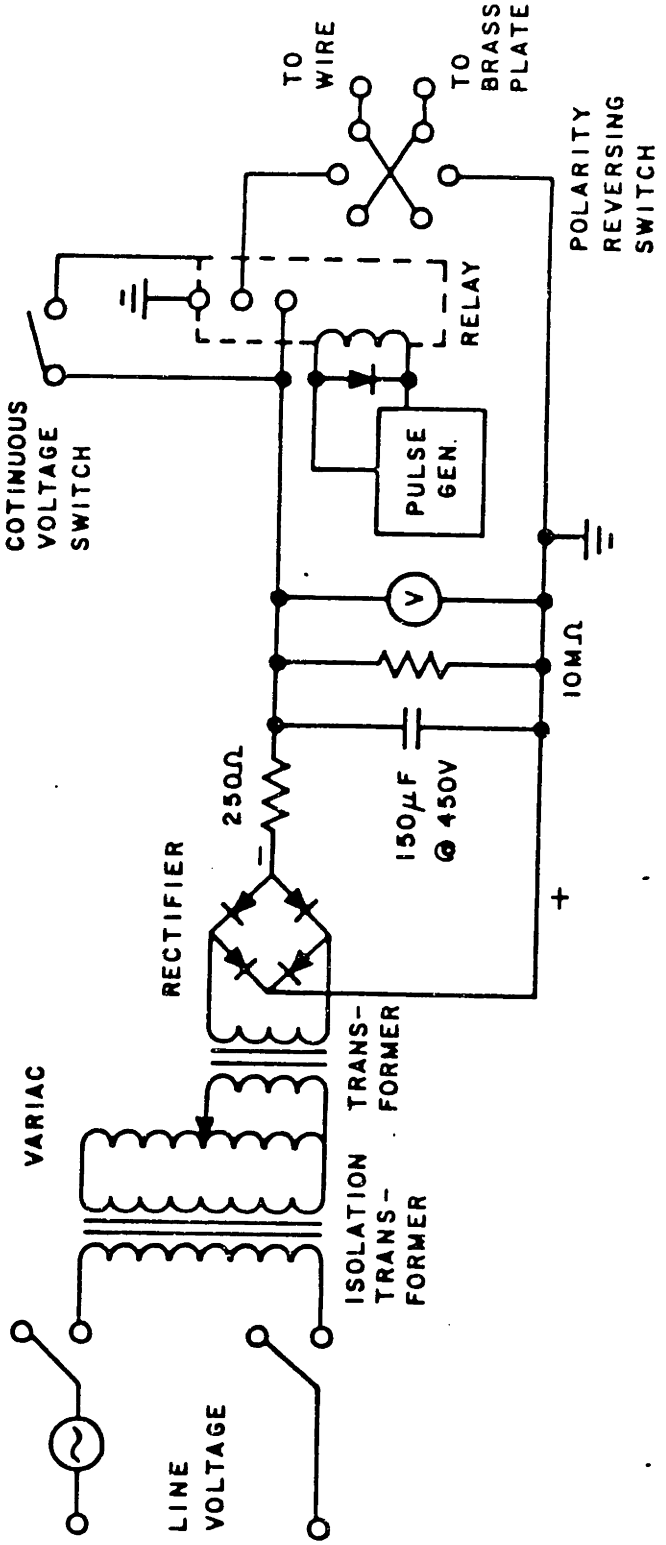

FIGURE 3-1: Hydrogen Bubble Flow Visualization DC Circuit

REFERENCES

1. Viguier, H.C., "A Secondary Flow Approach to the Inl Vortex Flow Field", MIT Gas Turbine Laboratory, Repc No. 155, 1980.

2. Feynman, R.P. and Leighton, R.B. and Sands, M., "The Flow of Dry Water", The Feynman Lectures on Physics, Volume II, Addison-Wesley Publication Co.,Mass., 197

3. Shapiro, A.H., "Vorticity", Illustrated Experiments Fluid Mechanics, The MIT Press, Mass., 1978.

4. Kerwin, J.E., "Variable Press Water Tunnel", MIT Department of Naval Architecture, Mass., 1967.

5. Kotansky, D.R., "Thin Airfoils in Rotational Flow", Gas Turbine Laboratory, Report No. 80, 1965.

6. Schraub, F.A., et al., "Use of Hydrogen Bubbles for Quantitative Determination of Time Dependent Velocit Fields in Low Speed Water Flows", Report MD-10, Ther sciences Division, Department of Mechanical Engineer Stanford University, 1964.

7. Clutter, D.W., et al., "Techniques of Flow Visualiza Using Water as the Working Medium", Douglas Aircraft Company Report ES-29075, 1959.

8. Mattingly, G.E., "The Hydrogen-Bubble Flow Visualiza Technique", David Taylor Model Basin Report 2146, 19

9. Bearman, P.W., and Zdravkovich, M.M., "Flow Around a Circular Cylinder Near a Plane Boundary", Journal of Fluid Mechanics, Vol. 89, 1978, pp. 33-47.

10. Marble, F.E., private communication.